Neuron-specific transcriptomic signatures indicate neuroinflammation and altered neuronal activity in ASD temporal cortex

Pan Zhang[1,2,3], Alicja Omanska[4,5], Bradley P. Ander[5,6], Michael J. Gandal[1,2,3*], Boryana Stamova[5,6*], Cynthia M. Schumann[4,5*]

Affiliations:

[1] Department of Psychiatry and Biobehavioral Sciences, David Geffen School of Medicine, University of California, Los Angeles, Los Angeles, CA, USA

[2] Department of Human Genetics, David Geffen School of Medicine, University of California, Los Angeles, Los Angeles, CA, USA

[3] Semel Institute for Neuroscience and Human Behavior, University of California, Los Angeles, Los Angeles, CA, USA

[4] Department of Psychiatry and Behavioral Sciences, University of California, Davis, School of Medicine, Sacramento, CA, USA

[5] University of California, Davis, MIND Institute, Sacramento, CA, USA

[6] Department of Neurology, University of California, Davis, School of Medicine, Sacramento, CA, USA

* Corresponding/Senior authors: Cynthia M. Schumann (cschumann@ucdavis.edu); Boryana Stamova (bsstamova@ucdavis.edu); Michael J. Gandal (mgandal@mednet.ucla.edu).

Abstract

Autism spectrum disorder (ASD) is a highly heterogeneous disorder, yet transcriptomic profiling of bulk brain tissue has identified substantial convergence among dysregulated genes and pathways in ASD. However, this approach lacks cell-specific resolution. We performed comprehensive transcriptomic analyses on bulk tissue and laser-capture microdissected (LCM) neurons of 59 postmortem human brains (27 ASD and 32 matched controls) in the superior temporal gyrus (STG) ranging from 2-73 years of age. In bulk tissue, synaptic signaling, heat shock protein-related pathways and RNA splicing were significantly altered in ASD. There was age-dependent dysregulation of genes involved in GABA (*GAD1* and *GAD2*) and glutamate (*SLC38A1*) signaling pathways. In LCM neurons, AP-1 mediated neuroinflammation and insulin/IGF-1 signaling pathways were upregulated in ASD, while mitochondrial function, ribosome and spliceosome components were downregulated. GABA synthesizing enzymes *GAD1* and *GAD2* were both downregulated in ASD neurons. Alterations in small nucleolar RNAs (snoRNAs) associated with splicing events suggested interplay between snoRNA dysregulation and splicing disruption in neurons of individuals with ASD. Our findings supported the fundamental hypothesis of altered neuronal communication in ASD, demonstrated that inflammation was elevated at least in part in ASD neurons, and may reveal windows of opportunity for biotherapeutics to target the trajectory of gene expression and clinical manifestation of ASD throughout the human lifespan.

Introduction

Autism spectrum disorder (ASD) defines a heterogeneous set of complex neurodevelopmental disorders affecting 1 in 54 children in the United States according to current estimation (1, 2)

and confers lifelong challenges. ASD is characterized by difficulties with social communication as well as a repetitive, restricted repertoire of behaviors and interests (3). Population, family and twin studies all indicate a strong genetic component contributing to risk for ASDs (4, 5), with heritability estimates of ~ 70% (6). However, the genetic causes and pathophysiology of ASD are varied and often complex.

Despite this heterogeneity, transcriptomic analyses of postmortem human brain have elucidated substantial convergent molecular-level pathology associated with idiopathic and syndromic forms of ASD (7-13). Multiple studies have profiled the transcriptomes of postmortem brain regions from individuals diagnosed with ASD (7, 8, 11, 14), including the temporal cortex implicated due to its critical importance in speech and language function (7, 8, 11). The most consistent findings include disruption of neuronal/synaptic activity and activation of innate immunity/glial markers (7, 8, 11). Dysregulation of alternative splicing and non-coding RNAs has also been shown to be dysregulated in ASD brains (8).

Most previous transcriptomic studies, however, profiled homogenate brain tissue and have therefore been unable to pinpoint the underlying specific cell-types in which gene expression is altered. Recently, Velmeshev *et al.* have published the first single-nucleus RNA-sequencing (sn-RNAseq) dataset in postmortem ASD cortex (13), identifying substantial changes in upper-layer excitatory neurons and microglia, consistent with observations from bulk tissue. As such sn-RNAseq datasets currently profile only the 3' end of highly expressed genes within each cell, these data characterize neither lowly expressed coding and non-coding genes, nor splicing alterations that may contribute to altered neuronal function in ASD.

Here, we performed the first systematic study using transcriptomic profiling to directly compare both bulk cortical tissue and laser capture microdissected (LCM) neurons from anatomically well-defined superior temporal gyrus (STG) samples from 59 subjects (27 with ASD and 32 age-

matched controls) ranging from 2-73 years of age (Figure 1, Supplementary Table 12). The STG modulates language processing and social perception, thereby playing a critical role in integrating a breadth of information to provide meaning to the surrounding world (15). Structural and functional imaging studies have long implicated STG in ASD (15, 16), however molecular-level changes in neurons remain unknown. This study aimed to identify neuron-specific transcriptomic changes in ASD brain by identifying differentially expressed genes, differential splicing events, age-related gene expression changes across the lifespan, as well as co-expression networks to reveal gene modules altered in ASD (Figure 1).

Results

Global gene expression changes in ASD superior temporal gyrus (STG)

RNA sequencing was performed on bulk tissue STG of 59 human brains, 27 from individuals with ASD and 32 from age-matched neurotypical controls, ranging from 2-73 years of age. Following quality control, we performed a comprehensive characterization of differential gene expression and local splicing alterations in ASD. After adjusting for known covariates and correcting for multiple comparisons, we found 194 differentially expressed genes between individuals with ASD and controls (FDR < 0.05). Of these, 143 were upregulated and 51 were downregulated (Figure 2A, Supplementary Table 1), with a median absolute fold change of 1.45 (range 1.11 - 4.04, Figure 2A). We observed significant concordance between our differential gene expression (DGE) results and previous data of the same region from different samples (12) (Supplementary Figure 1, Spearman $\rho = 0.37$ for t statistics, p-value < 10^{-16}).

Functional and pathway enrichment analyses indicated an over-representation of heat shock proteins (HSPs) and HSP-related chaperones, which were upregulated in ASD subjects. This included HSP70 family members *HSPA1A* and *HSPA1B*; HSP40 family members *DNAJB1* and

92 *DNAJB4*; small HSP20 family members *HSPB1* and *HSPB8*; and HSP-binding chaperons *BAG3*
93 and *PTGES3* (Figure 2C,D). HSPs are involved in stress-response, immune activation and
94 inflammation(17, 18), all of which were upregulated in ASD postmortem brain (7). Downregulated
95 genes were mainly enriched in pathways related to synaptic function (Figure 2D), consistent with
96 previous findings (7). Notably, two important voltage-gated potassium channel-related genes
97 *KCNH3* and *KCNIP1* were among the most downregulated (Figure 2C), which may relate to
98 disrupted neuronal excitability hypothesized in ASD (19, 20).

99 As age-dependent expression alterations have been reported in ASD brain (14), we employed an
100 analytical model accounting for age and the interaction between age and diagnosis. Fourteen
101 genes showed age-dependent DGE between ASD and control (Supplementary Table 2).
102 Interestingly, genes involved in gamma aminobutyric acid (GABA) synthesis (*GAD1* and *GAD2*)
103 (21) were downregulated in ASD only during late adulthood (Figure 2E). This may indicate an
104 age-dependent dysregulation of GABA signaling in ASD neurons, or a decrease in the proportion
105 of GABAergic neurons in ASD brains (22).

106 Differential splicing (DS) events in the bulk tissue transcriptome were evaluated using LeafCutter
107 (26). Among 35,505 intron clusters identified by LeafCutter, 308 clusters (297 unique genes)
108 showed significant DS between ASD patients and controls (FDR < 0.05). The 297 genes did not
109 show significant functional enrichment (Figure 2F, Supplementary Table 5).

110 To place subtle changes across the ASD STG transcriptome into a systems-level context, we
111 performed weighted gene correlation network analysis (WGCNA) to build gene co-expression
112 networks (23), identifying 31 modules of co-expressed genes (Methods; Supplementary Table 3).
113 Seven modules showed a significant association with ASD diagnosis, two of which were strongly
114 enriched for ASD-associated genetic risk factors (Modules Block-M1 and Block-M10, Figure 2B).

Module Block-M1 was upregulated in ASD STG and its gene members were enriched in RNA splicing and mRNA metabolic pathways (Supplementary Table 4). Notably, significantly upregulated HSPs were also members of the Block-M1 module (Supplementary Table 3). HSPs contribute to RNA splicing during stress (24). Downregulated modules in ASD were mostly enriched for synaptic functions (Block-M3, Block-M10, Block-M14, Block-M19, Block-M31; Supplementary Table 4). Cell-type enrichment analysis also indicated these downregulated modules were enriched in marker genes for both excitatory and inhibitory neurons (Figure 2B), suggesting a broad disruption of neuronal and synaptic processes in ASD STG.

Genes in the upregulated module Block-M1 and one downregulated module (Block-M10) were enriched in high-confidence ASD risk loci (25, 26), mutationally constrained (27) and highly intolerant to mutations (pLI > 0.99) genes (28), as well as regulatory target genes of CHD8, which has clear links to at least a subset of ASD cases (29) (Figure 2B). Many hub genes for module Block-M10 encoded synaptic proteins (Supplementary Figure 2, Supplementary Table 3). This module was also enriched for ASD common risk alleles from ASD GWAS data (30). Together this suggested a causal role of synaptic dysfunction in ASD etiology.

Neuron-specific gene expression and splicing alterations in ASD STG

To provide cell-type specificity for the observed transcriptomic changes, we next performed laser capture microdissection to capture neurons using STG sections taken from the same subjects profiled using bulk RNA-seq. We then interrogated ASD-associated gene expression and splicing alterations using the same bioinformatic pipelines as above. Across 13,458 neuron-expressed genes, 83 were significantly differentially expressed between ASD subjects and controls at FDR < 0.05, of which 52 were upregulated and 31 downregulated (Figure 3A, Supplementary Table 6). Median absolute fold change in expression between subjects with ASD and controls was 2.48 (range 1.29 - 9.72; Figure 3A). Surprisingly, concordance of neuronal DGE with bulk tissue DGE

was low (Spearman ρ = 0.18 for t statistics, Supplementary Figure 3), suggesting our analysis captured ASD signatures unique to neurons.

Upregulated genes in ASD neurons were highly enriched in pathways related to growth and differentiation (Figure 3E). Specifically, the AP-1 transcription factor complex components (31) *FOS*, *JUN* and *JUNB* were all up-regulated in ASD neurons, among other growth/differentiation regulators such as *SOX9*, *S1PR1* and *PPP1R16B* (Figure 3D). The AP-1 transcription factor complex is known to regulate a number of downstream biological processes (31). Indeed, we found upregulated B cell signaling adaptor gene *BCL10* and NFκB inhibitor delta gene *NFKBID* in ASD neurons (Figure 3D). NFκB and AP-1 may function together in regulating inflammatory processes (32-34), and up-regulation of both *NFKBID* and AP-1 point to dysregulated inflammation in ASD neurons. In addition, the inward-rectifier potassium ion channel gene *KCNJ2* was also up-regulated in ASD neurons (Figure 3D). Interestingly, both *KCNJ2* and AP-1 subunit *FOS* were involved in regulating excitability and plasticity at the cholinergic synapse (35-37).

Downregulated genes in ASD neurons are primarily enriched in mitochondrial function and oxidoreductase activity (Figure 3E). Specifically, comparing to bulk tissue STG, more subunits of the NADH:ubiquinone oxidoreductase (complex I) were downregulated in neurons, and their effect sizes were larger (Supplementary Figure 4). Indeed, oxidative phosphorylation (OXPHOS) defects have been reported in ASD lymphocytes, muscle, and temporal lobe (38-40). Our results provide evidence that compared to bulk tissue, mitochondrial dysfunction is much more profound in STG neurons.

While LCM captured both excitatory and inhibitory neurons, we note that *GAD1* and *GAD2* genes are among the most downregulated in ASD neurons (Figure 3D). The coordinated down-regulation of both GABA synthesizing enzymes suggest that the level of GABA neurotransmitter

may be decreased in ASD neurons, providing support to the excitation to inhibition (E/I) imbalance hypothesis of ASD (19, 20, 41).

By testing the interaction between diagnosis and age, 3 genes (*HTRA2,* aka *OMI*; *ZNF765*; and *PCDHB18P*) showed age-dependent differential expression in ASD neurons (Supplementary Table 7). For example, age trajectories of serine peptidase *HTRA2* were opposite in ASD brains compared to controls (Figure 3B). In healthy brains, the expression of *HTRA2* was much higher before age 30 and decreases with age, while its expression levels begin lower and increase with age in ASD STG neurons. Attenuated *HTRA2* activity may lead to neuronal cell death, altered chaperon activity and autophagy and has been linked to Parkinson's disease (42). In addition, increased active form of the *OMI/HTRA2* serine protease has been positively correlated with cholinergic alterations in AD brain (43). Thus, it is plausible that the altered expression of *HTRA2* with age we observed in ASD brain may be associated with neuronal alterations during development.

We also quantified local splicing events in the neuronal transcriptome. After adjusting for multiple testing, LeafCutter identified 1292 significant differential spliced intron clusters (1177 unique genes) out of 17,250 total intron clusters at FDR < 0.05 (Figure 3C, Supplementary Table 8). No functional enrichment was observed for the 1177 genes. We observed more disruptions in local splicing events in ASD neurons than in bulk tissue (308 DS out of 35505 events in bulk tissue, 1292 DS out of 17250 events in neurons; $p < 2 \times 10^{-16}$ test of proportions).

Neuron-specific networks pinpoint subtle changes in the neuronal transcriptome in ASD

Co-expression network analysis on neuronal data identified 18 modules, each containing between 101 and 998 co-expressed genes (Supplementary Table 9). Four modules were significantly upregulated in ASD neurons, while one module was downregulated (Figure 4A).

The upregulated neu-M5 co-expression module was highly represented by the DGE analysis signal. Upregulated genes *JUN, JUNB, NFKBID* were all hub genes of neu-M5 module. Neu-M5 module also captured additional AP-1 subunits and interactors, such as *FOSL2* (44) and *IRF3* (34, 45). Neu-M5 module was enriched in immune response pathways, providing further evidence that AP-1 mediated neuroinflammation was elevated in ASD neurons (Figure 4C, Supplementary Table 10). Hubs of Neu-M5 also contained multiple ion channel-related genes, such as sodium ion channel gene *SCN1B*, potassium channel genes *KCNJ2* and *KCNJ10*, and solute carrier gene *SLC40A1* (Figure 4C, Supplementary Table 9). Coordinated upregulation of various ion channels suggested that membrane transport was activated in ASD neurons, consistent with heightened excitability. Neu-M5 was significantly overlapped with module M16 from *Voineagu et al. (7)*. M16 was also enriched in immune/inflammatory response and was up-regulated in ASD (7). Our data refined our understanding of the neuroinflammatory changes in ASD to include a neuronal component. Additionally, downregulated neu-M17 module was enriched in mitochondrial function and contained most differentially expressed mitochondrial genes, such as ATP synthase subunits *ATP5F1B* and *ATP5PF* (Figure 4F, Supplementary Table 9).

Neuronal co-expression networks further captured signals that were not detected by DGE analysis. Neu-M6 module was upregulated in ASD, and among its hub genes were several insulin signaling pathway components, including insulin-like growth factor (IGF) receptor *IGF1R*, IGF binding protein *IGFBP5*, insulin receptor substrate *IRS2* as well as CBL-associated *SORBS1* (Figure 4D, Supplementary Table 9). Insulin signaling is associated with multiple neurodevelopmental disorders, including monogenetic ASD syndromes such as Rett and Phelan-McDermid syndromes (46-49). Our results provided direct molecular-level evidence that insulin signaling was altered in ASD neurons.

Among all five significantly disrupted modules, none were enriched for ASD common variants and only one upregulated module (Neu-M16) showed enrichment in highly confident ASD risk genes,

as well as in several other curated gene sets (Figure 4A). Neu-M16 was enriched in synaptic functions (Figure 4E, Supplementary Table 10). Further, cell-type analysis showed that Neu-M16 was also highly enriched in excitatory neurons (Figure 4B), with *CAMK2A* and *CAMK2B* among its hub genes (Supplementary Table 9). The upregulation of Neu-M16 suggested elevated excitatory signal in ASD neurons.

We further tested if significantly disrupted neuronal modules were enriched in any neuron subtypes. Upregulated neuronal modules in ASD were only enriched in excitatory neuron subtypes while enrichment of inhibitory neurons was only observed for downregulated modules (Figure 4B). This provides additional evidence for altered neuronal activity in ASD neurons, consistent with the findings in our DGE analysis.

Small non-coding RNAs are selectively down-regulated in ASD neurons and correlate with altered local splicing

When investigating the genes downregulated in ASD neurons more closely, we noticed a striking pattern that, 51 out of the 59 neuron-expressed small nucleolar RNA (snoRNA) (50) genes were down-regulated in ASD neurons, and 13 were significantly down-regulated at p-value < 0.05 (Figure 5A, Supplementary Table 6). Dysregulation of snoRNAs was not observed in bulk tissue (Supplementary Table 1), and snoRNAs were undetectable in a recent ASD single-cell study (13). snoRNAs are involved in the modification and maturation of ribosomal RNAs (rRNAs) and small nuclear RNAs (snRNAs) (51). Interestingly, both ribosome and spliceosome components were among the most downregulated in ASD neurons (Figure 3E). Moreover, snRNAs were also downregulated in ASD neurons, with 23 out of 24 snRNA genes down-regulated in ASD and 13 significantly down-regulated at p-value < 0.05 (Supplementary Figure 5, Supplementary Table 6).

As snoRNAs and snRNAs are known to be critical regulators of alternative splicing (52-55), and splicing alterations are strongly implicated in ASD and observed in LCM-captured neurons, we next examined alterations in splicing events that may be associated with snoRNA dysregulation. We calculated the correlation between snoRNA expression level and each local splicing event in neuronal data, followed by FDR correction for multiple comparisons. We identified 835 gene loci in neurons with at least one intron whose percent spliced in (PSI) was significantly correlated with snoRNA gene expression (Supplementary Table 11). Of these 835 intron clusters, 196 were significantly dysregulated in ASD neurons (Supplementary Table 11). Several intron clusters correlated with multiple snoRNAs and corresponded to genes involved in synaptic functions (Figure 5B). For example, *GOT1* encodes the glutamic-oxaloacetic transaminase known to function as an important regulator of glutamate level (56). PSI of intron 5 of *GOT1* was highly correlated with the expression level of multiple snoRNA genes (Figure 5C). *GOT1* intron 5 was also differentially spliced between ASD and control (Figure 5D). Differential splicing of *GOT1* gene may change the level of glutamate, and thus leads to an imbalance of E/I in neuronal communication in ASD neurons.

Discussion

Altered neuronal processes and synaptic function are consistent findings in transcriptomic analyses of ASD brain (7, 8, 11). However, transcriptomic studies of autistic brains are mostly limited to bulk tissue (7, 8, 11). Cell-type-specific molecular alterations in neurons are still largely unexplored. A recent single-cell RNA-seq study sheds light on the cell-type-specific transcriptomic changes in ASD (13), however, due to technology limitations, single-cell studies currently cannot reliably quantify low-expressed genes and local splicing events. Thus, in this study, we performed comprehensive analyses of gene expression and alternative splicing by short-read paired-end

RNA-seq on both bulk tissue and LCM-isolated neurons from the STG brain region in a cohort of 59 human brains ranging from 2-73 years of age.

Bulk tissue transcriptome findings reveal downregulated neuronal and synaptic function processes, upregulation of heat shock proteins, and unfolded protein response in ASD temporal cortex

Our bulk tissue analyses revealed a potential causal role of downregulated neuronal processes and synaptic functions in ASD etiology, consistent with findings from previous bulk-tissue transcriptomic studies on the same brain region (7). Previous studies also reported dysregulated alternative splicing events in ASD brain (8, 57). Differential splicing analysis in bulk STG found several synaptic genes, including *CANCA2D1*, *CAMK4*, *CLASP2*, *CNTNAP1*, *EPHB1*, *KALRN*, *NRXN3*, *SOS2* and *SYNGAP1*, differentially spliced in ASD. *SYNGAP1* isoforms have been shown to differentially regulate synaptic plasticity and dendritic development (58). This further signifies the importance of studying alternatively spliced isoforms in ASD brain.

We also observed a coordinated upregulation of multiple HSPs and HSP-related chaperones in ASD STG. HSPs can serve as activators and regulators of the immune system (18), and upregulated HSPs may induce immune responses in ASD brain. They also play a role in facilitating alternative RNA splicing (24). Previous studies found that both immune response and RNA splicing are upregulated in ASD brain (7, 8, 11), and our results signify that upregulated HSP-related pathways are a potential contributor to these observations. HSPs and HSP-related chaperones are normally induced in response to stress. The upregulation of HSPs in ASD neurons may relate to elevated endoplasmic reticulum (ER) stress since both unfolded protein response (UPR) and apoptosis are also upregulated in our ASD bulk data (Figure 2D). ASD-linked rare or *de novo* mutations in synaptic genes can lead to misfolded proteins and cause ER stress (59), itself coupled to heightened inflammation and neurotoxic cell death (60). ER stress-related

279 genes are also dysregulated in the middle frontal cortex of subjects with ASD (61). Our data
280 suggest that ER stress serves as a major response to ASD genetic mutations, and ER stress
281 activates UPR, including the production of HSPs and chaperones. UPR further induces multiple
282 downstream processes such as inflammation and immune response (62). Limiting the effect of
283 ER stress and UPR may be a promising therapeutic avenue for ASD.

284 **ASD neuronal transcriptome reveals upregulated neuroinflammation and altered**
285 **neuronal activity**

286 We observed a strong upregulation of AP-1 transcription factor components in ASD neurons. AP-
287 1 subunits *FOS*, *JUN* and *JUNB* were upregulated at FDR < 0.05, and *FOSL2* was upregulated
288 at nominal $p < 0.05$. AP-1 regulated gene expression in response to a variety of stimuli, including
289 cytokines, growth factors, stress signals, infections and inflammation/neuroinflammation (31). In
290 ASD neurons, it is likely that AP-1 activation induces broad inflammatory response, since several
291 immune and inflammation-related genes were also strongly upregulated. These included *NFKBID*
292 and *BCL10*, both of which were involved in the NF-κB pathway and were upregulated at FDR <
293 0.05. In addition, the interferon regulatory factor *IRF3* is upregulated at $p < 0.05$, and *IRF3* is co-
294 expressed with AP-1 subunits. The simultaneous upregulation of AP-1 subunits, NFκB-related
295 genes and interferon regulatory factors suggested that immune and inflammation responses were
296 activated in ASD neurons. Upregulated immune response and neuroinflammation have been
297 consistently observed in ASD patients by bulk tissue transcriptomic studies largely implicating
298 glial cells (7, 8). However, our results demonstrated that immune/neuroinflammatory response
299 was clearly activated in ASD neurons, and may be mediated by transcription factor AP-1. In
300 addition, analysis of the potential upstream regulators of the observed changes in the ASD
301 neuronal transcriptome with Ingenuity Pathway Analysis predicted their activation. This includes

MTORC2 member *RICTOR*, growth factors *FGF2* and *BMP4*, and *OSM* cytokine, most of which were implicated in ASD (63).

We also observed strong downregulation in ASD STG neurons of *GAD1* and *GAD2* genes, involved in the biosynthesis of the inhibitory neurotransmitter GABA. In contrast, *CAMK2A* and *CAMK2B* genes, which are essential for aspects of plasticity at glutamatergic excitatory synapses, are upregulated at nominal significance. In addition, co-expressed gene modules that were upregulated in ASD neurons were mainly enriched in excitatory neurons, while the downregulated module was primarily enriched in inhibitory neurons. These data provided further support for the hypothesis that ASD reflects imbalance of E/I in neuronal communication, also reported in several brain regions in ASD (19, 20, 41). To our knowledge this is the first report providing molecular-level evidence for imbalance of E/I in neuronal communication specifically in STG neurons in ASD.

Multiple insulin signaling pathway components, such as *IGFBP5*, *IRS2* and *SORBS1*, are coordinately upregulated in ASD neurons. Insulin signaling pathway is implicated in several neurodevelopmental disorders, likely due to its role in protein homeostasis and synaptic plasticity (46-49). Although the insulin-like peptide IGF-1 is currently in clinical trial for ASD, the direction of change in ASD brain is still controversial (49). In our data, the expression level of IGF-1 is downregulated in ASD neurons at nominal significance; upregulation of the aforementioned insulin signaling pathway components may reflect a compensatory reaction to the lack of IGF-1 ligand.

Future studies will focus on the role of snoRNAs in ASD neurons, as well as other long and small modulatory non-coding RNAs. Given the emerging role of snoRNAs as alternative splicing regulators (54, 55), we hypothesize that a coordinated downregulation of multiple snoRNAs correlates with elevated dysregulation of local splicing events in ASD neurons. Our data provide evidence supporting this hypothesis, however no causal relationship can be determined. It will be

326 critical to determine if snoRNA dysregulation plays a causal role in ASD etiology, and if so,
327 pinpoint the underlying mechanism and possibly relate to transcript isoforms driving ASD brain
328 and neuronal phenotype.

329 **Age-associated differential expression in STG points to altered neuronal activity in ASD**

330 Age-dependent gene expression changes have been observed in the ASD brains (64, 65). We
331 previously reported age-dependent miRNA alterations in the superior temporal sulcus (STS) and
332 adjacent primary auditory cortex (PAC) (64). In this study, a number of genes show varying age
333 trajectories in ASD bulk tissue and isolated neurons.

334 In bulk tissue, genes involved in GABAergic signaling (*GAD1* and *GAD2*) were upregulated with
335 age in controls, while downregulated with age in ASD. Multiple lines of evidence have pointed to
336 reduced neuronal inhibitory signal as a hallmark of ASD, including decreased number of
337 GABAergic interneuron (especially Parvalbumin neurons) (66) and reduced density of GABA
338 receptors (67-70). These cellular phenotypes are mainly observed in adults. Our findings
339 indicated that the reduction of *GAD1* and *GAD2* mRNA levels in ASD brain became more
340 profound with increasing age, consistent with the observations at cellular level. In addition,
341 *SLC38A1*, involved in neurotransmission at glutaminergic and GABAergic synapses (71), was
342 downregulated in ASD relative to control STG. *SLC38A1* is implicated in Rett Syndrome (72) and
343 mitochondrial disorders, and its decrease may contribute to the observed alterations in synapse
344 formation and neural connectivity.

345 In LCM neurons, the expression of *HTRA2* was higher below age 30 and decreases with age in
346 control neurons, while lower at younger ages and increasing with age in ASD neurons. HTRA2 is
347 important in maintaining mitochondrial homeostasis (73) and inducing apoptosis. It is implicated
348 in pathogenesis of neurodegeneration, hypoxic-ischemic damage, and is proposed as a potential
349 treatment target in neurological diseases (74). These findings further support the hypothesis of

350 altered neuronal E/I activity, neuroinflammation, cell death, and mitochondrial dysfunction,
351 implicated in ASD (75) and suggest treatment windows to target specific genes to alter their
352 expression trajectories with age.

353 **Closing**

354 Our study examined both bulk cortical tissue and isolated neurons from STG of autism and
355 control brain. We found expression patterns in neurons that are not detectable when aggregate
356 transcriptomes of multiple cells are profiled. In both cases, transcriptomic evidence suggested
357 alteration in E/I balance could contribute to asynchronous activity in the brain which may be a
358 contributing factor to autism in early development. Neuronal transcriptomes revealed further and
359 more specific evidence of divergent activity and molecular signaling pathways. Future studies
360 will need to examine the roles of other cell types in the brain and their contribution to ASD
361 phenotype. As research into ASD continues to focus on more precise data, it is apparent that
362 the complexity of factors that produce an ASD phenotype are slowly becoming clearer. As
363 recent technologies are applied to the valuable collections of banked brain tissue, better
364 definitions of specific subsets of ASD will become possible.

365 # Figure Legend

366 **Figure 1 Overview of experiment design and data analysis pipeline**

367 **Figure 2 Transcriptomic difference between ASD cases and controls in bulk tissue STG.**

368 **A**, Distribution of fold-change of differential expression for 194 differentially expressed genes.
369 Case:control fold-changes for upregulated genes are plotted in gold (N = 143, positive values)
370 and control:case fold-changes for downregulated genes in blue (N = 51, negative values). **B**, Co-
371 expressed gene modules that were significantly disrupted in ASD. Modules were hierarchically

clustered by module eigengene. Module-diagnosis associations were shown on the right of each module (*FDR < 0.05). Additional enrichment analyses were also shown for each module, including: Enrichment for ASD GWAS common variants (30)(*FDR < 0.1); Enrichment for major CNS cell types(76)(*FDR < 0.05); Enrichment against literature-curated gene lists (*FDR < 0.05) including pre- and postsynaptic marker genes (77), genes with likely-gene-disruption (LGD) or LGD plus missense de novo mutations(DNMs) found in patients with neurodevelopmental disorders(78), genes with probability of loss-of-function intolerance (pLI) > 0.99 as reported by the Exome Aggregation Consortium (28), mutationally constrained genes(27), vulnerable ASD genes(79), CHD8 targets(29), FMRP targets (80), syndromic and highly ranked (1 and 2) genes from SFARI Gene database. Abbreviations: Per, pericytes; OPC, oligodendrocyte progenitor cells; InNeu, inhibitory neuron; ExcNeu, excitatory neuron; Oligo, oligodendrocytes; Endo, endothelial cells; Astro, astrocytes. **C**, Volcano plot showing significantly up- (gold) and down-regulated (blue) genes (FDR < 0.05). Genes discussed in the main text are colored red. **D**, Functional enrichment of differentially expressed genes in ASD cases compared to controls. Top ten significantly enriched up- and down-regulated categories were shown. Categories were ranked by normalized enrichment score (NES), and NES for down-regulated categories were set to negative for displaying purpose solely. The color of each dot reflects FDR-corrected q-value, and the size of each dot reflects the number of overlapped genes between our gene list and the corresponding GO category. **E**, Age trajectory of GAD1 (left) and GAD2 (right) gene expression, stratified by ASD diagnosis. **F**, Quantile-quantile plot of observed p-values vs expected p-values for differentially spliced intron clusters. Significant DS events (FDR < 0.05) were colored red, and overlapping gene names were labeled for top clusters.

Figure 3 Differential gene expression and differential splicing between ASD cases and controls in LCM neurons from STG.

A, Distribution of fold-change of differential expression for 83 differentially expressed genes. Case:control fold-changes for upregulated genes are plotted in gold (N = 52, positive values) and control:case fold-changes for downregulated genes in blue (N = 31, negative values). **B**, Age trajectory of HTRA2 gene expression, stratified by ASD diagnosis. **C**, Quantile-quantile plot of observed p-values vs expected p-values for differentially spliced intron clusters. Significant DS events (FDR < 0.05) were colored red, and overlapping gene names were labeled for top clusters. DS results from bulk tissue were also plotted for comparison. **D**, Volcano plot showing up- (gold) and down-regulated (blue) genes. Genes discussed in the main text are colored red. **E**, Functional enrichment of differentially expressed genes in ASD cases compared to controls. Top ten significantly enriched up- and down-regulated categories are shown. Categories were ranked by normalized enrichment score (NES), and NES for down-regulated categories were set to negative for display purposes solely. The color of each dot reflects FDR-corrected q-value, and the size of each dot reflects the number of overlapped genes between our gene list and the corresponding GO category.

Figure 4 Gene co-expression network analysis of the ASD neuronal transcriptome.

A, Hierarchical clustering of neuronal gene co-expression modules by module eigengenes. Module-diagnosis associations were shown below each module. Enrichment for ASD GWAS common variants is shown for each module. Enrichment against literature-curated gene lists is shown on the bottom. **B**, Module enrichment for neuron subtypes. Expression profiles of neuron subtypes were obtained from ref. (76). Red asterisks indicate significant enrichment. **C-F**, Functional enrichment (top panel) and top 50 hub genes (bottom panel) for module neu-M5 (C), neu-M6 (D), neu-M16 (E) and neu-M17 (F). Edges represent co-expression (Pearson correlation > 0.5). Co-expressed partners with evidence of protein-protein interaction were connected by solid

419 black lines. PPI data was compiled from well-characterized PPI databases, including Bioplex,
420 HPRD, Inweb, HINT, Biogrid, GeneMANIA, STRING and CORUM. Only physical interactions and
421 co-complex associations were kept.

422 **Figure 5 Coordinated dysregulation of snoRNAs in ASD neurons.**

423 **A**, Volcano plot showing differentially expressed genes in ASD neurons compared to control.
424 snoRNA genes were colored red. **B**, Significant correlation between snoRNA expression (x-axis)
425 and intron PSI (y-axis). Introns are labeled with the name of overlapping gene locus. Gene loci
426 that are correlated with more than 3 snoRNAs were shown. **C**, Scatter plot showing the correlation
427 between GOT1 intron 5 PSI and expression levels of multiple snoRNAs across all neuron samples.
428 Also shown were fitted regression lines with 95% confidence intervals. Intron coordinates were
429 based on GRCh37. **D**, PSI of GOT1 intron 5 is downregulated in ASD neurons.

430 **Supplementary Figure 1**

431 Binned density scatter plot comparing the t-statistics for case versus control differential
432 expression between this study and another study (De Bree *et al.*, unpublished) comparing gene
433 expression between ASD and controls in BA41, BA42, and BA22 bulk tissues; correlation
434 between the statistics is 0.37 ($P < 10^{-16}$).

435 **Supplementary Figure 2**

436 Representative genes in module Block-M10. Known ASD risk genes were colored red. Synaptic
437 genes that are intolerant to LOF mutation were colored pink. Edges represent co-expression.

Supplementary Figure 3

Binned density scatter plot comparing the t-statistics for case versus control differential expression between neurons and bulk tissue; correlation between the statistics is 0.18 ($P < 10^{-16}$).

Supplementary Figure 4

Fold changes (ASD *vs.* CTL) of NADH:ubiquinone oxidoreductase (complex I) subunits in block tissue (red) and neurons (green).

Supplementary Figure 5

Volcano plot showing differentially expressed genes in ASD neurons compared to control. snRNA genes were colored red.

Supplementary Table 1

DGE summary statistics for block tissue

Supplementary Table 2

DGE summary statistics for age-diagnosis-interaction in block tissue

Supplementary Table 3

Gene co-expression network module membership for block tissue

Supplementary Table 4

Gene co-expression network module functional enrichment for block tissue

Supplementary Table 5

DS summary statistics for block tissue

Supplementary Table 6

DGE summary statistics for LCM neuron

Supplementary Table 7

DGE summary statistics for age-diagnosis-interaction in LCM neuron

Supplementary Table 8

DS summary statistics for LCM neuron

Supplementary Table 9

Gene co-expression network module membership for LCM neuron

Supplementary Table 10

Gene co-expression network module functional enrichment for LCM neuron

Supplementary Table 11

Significant correlations between snoRNA gene expression and local splicing events

Supplementary Table 12

Donor information

Methods

Block tissue RNA extraction and library preparation

Human brain tissue was collected, sectioned coronally and flash frozen. STG from 32 controls and 27 ASD cases (2-73 years old) was identified anatomically according to "Atlas of the Human Brain" 4th edition (Maj, Majtanik, Paxinos 2015). Brain tissue (18-25 mg) was excised from the

476 STG and put directly into 600 µl of Tri Reagent lysis buffer. Total RNA was extracted using the
477 Direct-zol RNA MiniPrep (Zymo Research #R2051) following manufacturer's protocol, with the
478 inclusion of DNase I treatment and eluted in DNase/RNase-free water. Quality and quantity of
479 RNA were determined via RNA 6000 Nano chip on 2100 Bioanalyzer (Agilent), NanoDrop 2000
480 spectrophotometer (ThermoFisher Scientific), and Qubit fluorometer (ThermoFisher Scientific).

481 From each of the 48 STG samples, 50 ng of RNA were used to create strand-specific total RNA
482 libraries with the NuGEN Ovation Universal RNA-Seq System v2 and processed in parallel on the
483 Sciclone NGS automated workstation (Perkin Elmer) according to manufacturer protocol.
484 Following second-strand cDNA synthesis, samples were sheared by sonication on the Covaris
485 E220. InDA-C (aka AnyDeplete) primers were used to target and cleave adapters from rRNA
486 transcripts before amplification of libraries through 16 cycles of PCR. Final barcoded libraries
487 were bead purified and examined for QC using 2100 BioAnalyzer DNA High Sensitivity chips.
488 Library concentration was calculated based on fragment size and normalized to 15 nM for
489 sequencing.

490 **Laser capture microdissection, RNA extraction and library preparation**

491 Fresh-frozen STG tissue samples from 22 controls and 18 ASD cases (8-73 years old) were
492 carefully dissected and embedded in OCT compound. The specimens were sectioned on a
493 Microm HM550 cryostat (Thermo Scientific) at 12 µm and mounted on PEN membrane slides
494 (ThermoFisher Scientific #LCM0522). Sections were hydrated with an ice-chilled ethanol series
495 (100%, 75%, 50%) for 2 min each followed by HistoGene staining solution (ThermoFisher
496 Scientific #KIT0415) for 30 seconds, 2 rinses in nuclease-free water, and alcohol dehydration
497 (50%, 75%, 95%, 100% with molecular sieves). Slides were air dried and maintained on dry ice
498 until laser capture microdissection.

Using a Leica LMD-6000 laser capture microdissection system, 100 neurons from each sample were laser captured directly into lysis buffer (PicoPure RNA Isolation Kit, ThermoFisher Scientific KIT0204). RNA was extracted using the PicoPure total RNA kit with inclusion of DNase I digest according to manufacturer protocol.

Strand-specific rRNA depleted RNA libraries were prepared from 10 µl of the final neuronal RNA eluate using the NuGEN Ovation SoLo Kit (NuGen #0500) for ultra-low input following manufacturer protocol with final amplification of 18 PCR cycles. Barcoded bead purified libraries were examined for QC using Qubit Fluorometer (ThermoFisher Scientific) and 2100 BioAnalyzer DNA High Sensitivity chips. Library concentration was calculated based on fragment size and normalized to 15 nM for sequencing.

RNA sequencing

Library concentrations were confirmed with qPCR and pooled before RNA-Seq was performed on Illumina HiSeq4000 at the Vincent J. Coates Genomics Sequencing Laboratory at the California Institute for Quantitative Biosciences (QB3) at University of California, Berkeley. Libraries from LCM samples and STG blocks were sequenced to about 50 million 2x150bp reads per sample. For libraries prepared with the NuGEN Ovation SoLo kit a Custom R1 primer (NuGEN) was used in place of the standard Illumina forward read primer.

Mapping, quantification of gene expression, and QC

RNA-seq reads were aligned to the GRCH37.p13 (hg19) reference genome via STAR (2.7.2a) using comprehensive gene annotations from GENCODE (v29 lifted over to hg19). Gene-level quantifications were calculated using featureCounts (v1.6.4), considering only uniquely-mapped reads. Quality control metrics were calculated using PicardTools (v2.21.2).

Gene-level counts were compiled and imported into R for downstream analyses. Expressed genes were defined as genes with non-zero count in at least 80% of samples. A total of 22,729 and 13,458 expressed genes from block tissue and LCM neurons, respectively, were used in the downstream analysis. Sample outliers were defined as samples with standardized sample network connectivity Z scores < -2 (81), and were removed.

A set of 105 RNA-Seq quality control metrics from the outputs of PicardTools (CollectAlignmentSummaryMetrics, CollectInsertSizeMetrics, CollectRnaSeqMetrics, CollectGcBiasMetrics, MarkDuplicates) were compiled for each group of samples (block tissue and LCM neurons). These measures were summarized by the top principal components (termed seqPCs), which explained a significant portion of the total variance of each dataset. These seqPCs were used as potential covariates for downstream analysis.

Differential gene expression

Differential Gene Expression (DGE) analyses were performed using DESeq2 (1.22.2)(82) with default parameters. For block tissue data, diagnosis, sex, age, RNA integrity number (RIN), absorbance 260/280 ratio (A260/280) and top 3 seqPCs were used as covariates. For neuron data, diagnosis, sex, age, RNA library batch and top 3 seqPCs were used as covariates. To identify age-dependent differential expression, an interaction term between age and diagnosis was added to the above DESeq2 models.

Differential alternative splicing

Local splicing analysis was performed using LeafCutter(83) as previously described(10). In brief, Clusters of variable spliced introns across all samples were called first. Then differential splicing between ASD and control group was identified in each data set (bulk tissue and neuron) by jointly

545 modeling intron clusters using the Dirichlet-Multinomial generalized linear model (GLM). We
546 controlled for the same covariates as above in the DGE analysis.

547 Intron clusters were first filtered to only keep clusters supported by at least 50 split reads across
548 all samples, retaining introns of up to 100 kb and accounting for at least 1% of the total number
549 of reads in the entire cluster. This intron count file was then used in the differential splicing (DS)
550 analysis. For DS analysis, we further discarded introns that were not supported by at least one
551 read in 5 or more samples. Clusters were then analyzed for DS if at least 3 samples in each
552 comparison group (i.e. ASD or controls) had an overall coverage of 20 or more reads. P-values
553 were corrected for multiple testing using the Benjamini-Hochberg (BH) method and used to select
554 clusters with significant splicing differences (FDR < 0.1).

555 **Co-expression network analysis**

556 Weighted gene co-expression network analysis (WGCNA)(23) defined modules of co-expressed
557 genes from RNA-seq data. All covariates except for ASD diagnosis, sex and age were first
558 regressed out from the expression datasets. The co-expression networks and modules were
559 estimated using the blockwiseModules function with the following parameters: corType=bicorr;
560 networkType=signed; pamRespectsDendro=F; mergeCutHeight=0.1, power=8, deepSplit=2,
561 minModuleSize=40. Module eigengene/genotype associations were calculated using a linear
562 model. Significance p-values were FDR-corrected to account for multiple comparisons. Genes
563 within each module were prioritized based on their module membership (kME), defined as
564 correlation to the module eigengene. For selected modules, the top hub genes were shown.

565 **Functional enrichment analysis**

566 For co-expressed gene modules, enrichment for Gene Ontology (GO; Biological Process and
567 Molecular Function) was performed using gProfileR R package(84). Background was restricted

to the expressed set of genes. An ordered query was used, ranking genes by kME for WGCNA analyses.

For DGE, GO enrichment was performed using the GSEA algorithm as implemented in the clusterProfiler R package(85). All genes were ranked by log2 fold change.

Enrichment analyses were also performed using several established, hypothesis-driven gene sets including pre- and postsynaptic marker genes (77), genes with likely-gene-disruption (LGD) or LGD plus missense de novo mutations(DNMs) found in patients with neurodevelopmental disorders(78), genes with probability of loss-of-function intolerance (pLI) > 0.99 as reported by the Exome Aggregation Consortium (28), mutationally constrained genes(27), vulnerable ASD genes(79), CHD8 targets(29), FMRP targets (80), syndromic and highly ranked (1 and 2) genes from SFARI Gene database. Statistical enrichment analyses were performed using permutation test. One thousand simulated lists with similar number of genes, gene length distribution and GC-content distribution as the target gene list were generated, and the overlaps between each of the simulated list and the hypothesis-driven gene sets were calculated to form the null distribution. Significance p-value was calculated by comparing the actual overlap between target list and hypothesis-driven gene sets to the null distribution. All results were FDR-corrected for multiple comparisons.

Ingenuity pathway analysis

We performed Ingenuity Pathway Analysis (IPA®, QIAGEN) to identify significantly over-represented pathways and to determine if they are activated or inhibited in ASD brain compared to control brain. IPA predicts the overall direction of the pathway (activation or inhibition) using a Z-score to statistically compare our datasets with expression patterns in the IPA knowledge base (86). This is achieved by considering the activation state of key molecules when the

Pathway is activated and the molecules' causal relationships. $Z \geqslant 2$ signifies a pathway that is significantly activated, while $Z \leqslant -2$ - significantly suppressed in ASD compared to control brain.

Cell type enrichment analysis

Cell-type enrichment analysis for each co-expression module was performed using the Expression Weighted Cell Type Enrichment (EWCE) package in R(87). Cell type-specific gene expression data was obtained from single nucleus sequencing of adult human brains (88). The specificity metric of each gene for each cell type was computed as described(87). Enrichment was evaluated using bootstrapping. Z-score was estimated by the distance of the mean expression of the target gene set from the mean expression of bootstrapping replicates. P-values were corrected for multiple comparisons using FDR.

GWAS enrichment analysis

The most recent ASD GWAS summary statistics were obtained from Grove *et al.*(30) Stratified LD score regression (sLDSC)(89) was used to test whether a gene set of interest is enriched for SNP-heritability in a given GWAS dataset. In brief, SNPs were assigned to custom gene categories if they fell within ±100 kb of any gene in a set. These categories were added to a full baseline model that includes 53 functional categories capturing a broad set of genomic annotations. The MHC region was excluded from all analyses. Enrichment was calculated as the proportion of SNP-heritability accounted for by each category divided by the proportion of total SNPs within the category. Significance was assessed using a block jackknife procedure, followed by Bonferroni correction for the number of gene sets.

Data Availability

RNA-seq data will be submitted to the NCBI Sequence Read Archive (SRA), and accession code will be available before publication.

Code Availability

All custom code used in this manuscript is available at https://github.com/gandallab/ASD_STG_LCM_RNAseq

Acknowledgments

We are grateful to the families of our brain donors for their invaluable gift to autism research. We appreciate the contributions of Carolyn Komich Hare, clinical coordinator for BrainNet, for collection of the ADI-R as well as Robin Riedel, UC Davis, for figure design. Tissue was provided by the University of Maryland Brain and Tissue Bank, Dr. Daniel Campbell at Michigan State University, Autism Tissue Program (now Autism BrainNet, supported by the Simons Foundation), Brain Endowment for Autism Research Sciences (BEARS) at the UC Davis MIND Institute, and the Harvard Brain Tissue Resource Center. Laser capture microdissection was conducted using the CAMI core facility at UC Davis Center for Health and the Environment with instrumentation funding by NIHS10RR-023555. RNA sequencing was conducted using the Vincent J. Coates Genomics Sequencing Laboratory at UC Berkeley, supported by NIH S10 OD018174 Instrumentation Grant. This work is supported by NIH grants MH108909 (MPI Schumann, Stamova) and the Intellectual and Developmental Disabilities Research Center at UC Davis (1U54HD079125).

Author Contributions

C.M.S., B.S. and B.P.A. conceived the project. C.M.S., B.S. and M.J.G. supervised the study. A.O., B.P.A., B.S. and C.M.S. designed and performed the experiments. P.Z., B.S. and M.J.G. designed and performed computational analyses. P.Z. wrote the paper with input from all co-authors.

Competing Interests

The authors declare no competing interests.

References

1. Kim YS, Leventhal BL, Koh Y-J, Fombonne E, Laska E, Lim E-C, et al. Prevalence of autism spectrum disorders in a total population sample. Am J Psychiatry. 2011;168(9):904-12.
2. Maenner MJ, Shaw KA, Baio J, EdS, Washington A, Patrick M, et al. Prevalence of Autism Spectrum Disorder Among Children Aged 8 Years - Autism and Developmental Disabilities Monitoring Network, 11 Sites, United States, 2016. MMWR Surveill Summ. 2020;69(4):1-12.
3. Lord C, Brugha TS, Charman T, Cusack J, Dumas G, Frazier T, et al. Autism spectrum disorder. Nat Rev Dis Primers. 2020;6(1):5.
4. Hansen SN, Schendel DE, Francis RW, Windham GC, Bresnahan M, Levine SZ, et al. Recurrence Risk of Autism in Siblings and Cousins: A Multinational, Population-Based Study. J Am Acad Child Adolesc Psychiatry. 2019;58(9):866-75.

654 5. Castelbaum L, Sylvester CM, Zhang Y, Yu Q, Constantino JN. On the Nature of
655 Monozygotic Twin Concordance and Discordance for Autistic Trait Severity: A Quantitative
656 Analysis. Behav Genet. 2020;50(4):263-72.
657 6. Gaugler T, Klei L, Sanders SJ, Bodea CA, Goldberg AP, Lee AB, et al. Most genetic risk
658 for autism resides with common variation. Nat Genet. 2014;46(8):881-5.
659 7. Voineagu I, Wang X, Johnston P, Lowe JK, Tian Y, Horvath S, et al. Transcriptomic
660 analysis of autistic brain reveals convergent molecular pathology. Nature. 2011;474(7351):380-
661 4.
662 8. Parikshak NN, Swarup V, Belgard TG, Irimia M, Ramaswami G, Gandal MJ, et al.
663 Genome-wide changes in lncRNA, splicing, and regional gene expression patterns in autism.
664 Nature. 2016;540(7633):423-7.
665 9. Gandal MJ, Haney JR, Parikshak NN, Leppa V, Ramaswami G, Hartl C, et al. Shared
666 molecular neuropathology across major psychiatric disorders parallels polygenic overlap.
667 Science. 2018;359(6376):693-7.
668 10. Gandal MJ, Zhang P, Hadjimichael E, Walker RL, Chen C, Liu S, et al. Transcriptome-
669 wide isoform-level dysregulation in ASD, schizophrenia, and bipolar disorder. Science.
670 2018;362(6420).
671 11. Gupta S, Ellis SE, Ashar FN, Moes A, Bader JS, Zhan J, et al. Transcriptome analysis
672 reveals dysregulation of innate immune response genes and neuronal activity-dependent genes
673 in autism. Nat Commun. 2014;5:5748.
674 12. Haney JR, Wamsley B, Chen GT, Parhami S, Emani PS, Chang N, et al. Broad
675 transcriptomic dysregulation across the cerebral cortex in ASD. bioRxiv.
676 2020:2020.12.17.423129.
677 13. Velmeshev D, Schirmer L, Jung D, Haeussler M, Perez Y, Mayer S, et al. Single-cell
678 genomics identifies cell type-specific molecular changes in autism. Science.
679 2019;364(6441):685-9.

680 14. Chow ML, Pramparo T, Winn ME, Barnes CC, Li H-R, Weiss L, et al. Age-dependent
681 brain gene expression and copy number anomalies in autism suggest distinct pathological
682 processes at young versus mature ages. PLoS Genet. 2012;8(3):e1002592.
683 15. Jou RJ, Minshew NJ, Keshavan MS, Vitale MP, Hardan AY. Enlarged right superior
684 temporal gyrus in children and adolescents with autism. Brain Res. 2010;1360:205-12.
685 16. Amaral DG, Schumann CM, Nordahl CW. Neuroanatomy of autism. Trends Neurosci.
686 2008;31(3):137-45.
687 17. Feder ME, Hofmann GE. Heat-shock proteins, molecular chaperones, and the stress
688 response: evolutionary and ecological physiology. Annu Rev Physiol. 1999;61:243-82.
689 18. Binder RJ. Functions of heat shock proteins in pathways of the innate and adaptive
690 immune system. J Immunol. 2014;193(12):5765-71.
691 19. Sohal VS, Rubenstein JLR. Excitation-inhibition balance as a framework for investigating
692 mechanisms in neuropsychiatric disorders. Mol Psychiatry. 2019;24(9):1248-57.
693 20. Nelson SB, Valakh V. Excitatory/Inhibitory Balance and Circuit Homeostasis in Autism
694 Spectrum Disorders. Neuron. 2015;87(4):684-98.
695 21. Grone BP, Maruska KP. Three Distinct Glutamate Decarboxylase Genes in Vertebrates.
696 Sci Rep. 2016;6:30507.
697 22. Patrick E, Taga M, Ergun A, Ng B, Casazza W, Cimpean M, et al. Deconvolving the
698 contributions of cell-type heterogeneity on cortical gene expression. PLoS Comput Biol.
699 2020;16(8):e1008120.
700 23. Langfelder P, Horvath S. WGCNA: an R package for weighted correlation network
701 analysis. BMC Bioinformatics. 2008;9:559.
702 24. Yost HJ, Lindquist S. RNA splicing is interrupted by heat shock and is rescued by heat
703 shock protein synthesis. Cell. 1986;45(2):185-93.

704 25. Satterstrom FK, Kosmicki JA, Wang J, Breen MS, De Rubeis S, An J-Y, et al. Large-
705 Scale Exome Sequencing Study Implicates Both Developmental and Functional Changes in the
706 Neurobiology of Autism. Cell. 2020;180(3):568-84.e23.
707 26. Abrahams BS, Arking DE, Campbell DB, Mefford HC, Morrow EM, Weiss LA, et al.
708 SFARI Gene 2.0: a community-driven knowledgebase for the autism spectrum disorders
709 (ASDs). Mol Autism. 2013;4(1):36.
710 27. Samocha KE, Robinson EB, Sanders SJ, Stevens C, Sabo A, McGrath LM, et al. A
711 framework for the interpretation of de novo mutation in human disease. Nat Genet.
712 2014;46(9):944-50.
713 28. Karczewski KJ, Weisburd B, Thomas B, Solomonson M, Ruderfer DM, Kavanagh D, et
714 al. The ExAC browser: displaying reference data information from over 60 000 exomes. Nucleic
715 Acids Res. 2017;45(D1):D840-D5.
716 29. Wilkinson B, Grepo N, Thompson BL, Kim J, Wang K, Evgrafov OV, et al. The autism-
717 associated gene chromodomain helicase DNA-binding protein 8 (CHD8) regulates noncoding
718 RNAs and autism-related genes. Transl Psychiatry. 2015;5:e568.
719 30. Grove J, Ripke S, Als TD, Mattheisen M, Walters RK, Won H, et al. Identification of
720 common genetic risk variants for autism spectrum disorder. Nat Genet. 2019;51(3):431-44.
721 31. Hess J, Angel P, Schorpp-Kistner M. AP-1 subunits: quarrel and harmony among
722 siblings. J Cell Sci. 2004;117(Pt 25):5965-73.
723 32. Gehring T, Seeholzer T, Krappmann D. BCL10 - Bridging CARDs to Immune Activation.
724 Front Immunol. 2018;9:1539.
725 33. Ji Z, He L, Regev A, Struhl K. Inflammatory regulatory network mediated by the joint
726 action of NF-kB, STAT3, and AP-1 factors is involved in many human cancers. Proc Natl Acad
727 Sci U S A. 2019;116(19):9453-62.
728 34. Iwanaszko M, Kimmel M. NF-κB and IRF pathways: cross-regulation on target genes
729 promoter level. BMC Genomics. 2015;16:307.

730 35. Warburton EC, Koder T, Cho K, Massey PV, Duguid G, Barker GRI, et al. Cholinergic
731 neurotransmission is essential for perirhinal cortical plasticity and recognition memory. Neuron.
732 2003;38(6):987-96.
733 36. Binda A, Rivolta I, Villa C, Chisci E, Beghi M, Cornaggia CM, et al. A Novel KCNJ2
734 Mutation Identified in an Autistic Proband Affects the Single Channel Properties of Kir2.1. Front
735 Cell Neurosci. 2018;12:76.
736 37. Ambrosini E, Sicca F, Brignone MS, D'Adamo MC, Napolitano C, Servettini I, et al.
737 Genetically induced dysfunctions of Kir2.1 channels: implications for short QT3 syndrome and
738 autism-epilepsy phenotype. Hum Mol Genet. 2014;23(18):4875-86.
739 38. Siddiqui MF, Elwell C, Johnson MH. Mitochondrial Dysfunction in Autism Spectrum
740 Disorders. Autism Open Access. 2016;6(5).
741 39. Rossignol DA, Frye RE. Mitochondrial dysfunction in autism spectrum disorders: a
742 systematic review and meta-analysis. Mol Psychiatry. 2012;17(3):290-314.
743 40. Tang G, Gutierrez Rios P, Kuo S-H, Akman HO, Rosoklija G, Tanji K, et al.
744 Mitochondrial abnormalities in temporal lobe of autistic brain. Neurobiol Dis. 2013;54:349-61.
745 41. Rubenstein JLR, Merzenich MM. Model of autism: increased ratio of excitation/inhibition
746 in key neural systems. Genes Brain Behav. 2003;2(5):255-67.
747 42. Plun-Favreau H, Klupsch K, Moisoi N, Gandhi S, Kjaer S, Frith D, et al. The
748 mitochondrial protease HtrA2 is regulated by Parkinson's disease-associated kinase PINK1. Nat
749 Cell Biol. 2007;9(11):1243-52.
750 43. Darreh-Shori T, Rezaeianyazdi S, Lana E, Mitra S, Gellerbring A, Karami A, et al.
751 Increased active OMI/HTRA2 serine protease displays a positive correlation with cholinergic
752 alterations in the Alzheimer’s disease brain. Molecular neurobiology. 2019;56(7):4601-19.
753 44. Renoux F, Stellato M, Haftmann C, Vogetseder A, Huang R, Subramaniam A, et al. The
754 AP1 Transcription Factor Fosl2 Promotes Systemic Autoimmunity and Inflammation by
755 Repressing Treg Development. Cell Rep. 2020;31(13):107826.

45. Sweeney SE, Kimbler TB, Firestein GS. Synoviocyte innate immune responses: II. Pivotal role of IFN regulatory factor 3. J Immunol. 2010;184(12):7162-8.

46. Marchetto MCN, Carromeu C, Acab A, Yu D, Yeo GW, Mu Y, et al. A model for neural development and treatment of Rett syndrome using human induced pluripotent stem cells. Cell. 2010;143(4):527-39.

47. Shcheglovitov A, Shcheglovitova O, Yazawa M, Portmann T, Shu R, Sebastiano V, et al. SHANK3 and IGF1 restore synaptic deficits in neurons from 22q13 deletion syndrome patients. Nature. 2013;503(7475):267-71.

48. Marchetto MC, Belinson H, Tian Y, Freitas BC, Fu C, Vadodaria K, et al. Altered proliferation and networks in neural cells derived from idiopathic autistic individuals. Mol Psychiatry. 2017;22(6):820-35.

49. Vahdatpour C, Dyer AH, Tropea D. Insulin-Like Growth Factor 1 and Related Compounds in the Treatment of Childhood-Onset Neurodevelopmental Disorders. Front Neurosci. 2016;10:450.

50. Kiss T. Small nucleolar RNAs: an abundant group of noncoding RNAs with diverse cellular functions. Cell. 2002;109(2):145-8.

51. Bratkovič T, Božič J, Rogelj B. Functional diversity of small nucleolar RNAs. Nucleic Acids Res. 2020;48(4):1627-51.

52. Dvinge H, Guenthoer J, Porter PL, Bradley RK. RNA components of the spliceosome regulate tissue- and cancer-specific alternative splicing. Genome Res. 2019;29(10):1591-604.

53. Valadkhan S, Gunawardane LS. Role of small nuclear RNAs in eukaryotic gene expression. Essays Biochem. 2013;54:79-90.

54. Kishore S, Stamm S. The snoRNA HBII-52 regulates alternative splicing of the serotonin receptor 2C. Science. 2006;311(5758):230-2.

780 55. Falaleeva M, Pages A, Matuszek Z, Hidmi S, Agranat-Tamir L, Korotkov K, et al. Dual
781 function of C/D box small nucleolar RNAs in rRNA modification and alternative pre-mRNA
782 splicing. Proc Natl Acad Sci U S A. 2016;113(12):E1625-34.
783 56. D'Aniello A, Fisher G, Migliaccio N, Cammisa G, D'Aniello E, Spinelli P. Amino acids and
784 transaminases activity in ventricular CSF and in brain of normal and Alzheimer patients.
785 Neurosci Lett. 2005;388(1):49-53.
786 57. Stamova BS, Tian Y, Nordahl CW, Shen MD, Rogers S, Amaral DG, et al. Evidence for
787 differential alternative splicing in blood of young boys with autism spectrum disorders. Molecular
788 autism. 2013;4(1):1-16.
789 58. Araki Y, Hong I, Gamache TR, Ju S, Collado-Torres L, Shin JH, et al. SynGAP isoforms
790 differentially regulate synaptic plasticity and dendritic development. Elife. 2020;9:e56273.
791 59. Comoletti D, De Jaco A, Jennings LL, Flynn RE, Gaietta G, Tsigelny I, et al. The
792 Arg451Cys-neuroligin-3 mutation associated with autism reveals a defect in protein processing.
793 J Neurosci. 2004;24(20):4889-93.
794 60. Sprenkle NT, Sims SG, Sánchez CL, Meares GP. Endoplasmic reticulum stress and
795 inflammation in the central nervous system. Molecular neurodegeneration. 2017;12(1):1-18.
796 61. Crider A, Ahmed AO, Pillai A. Altered Expression of Endoplasmic Reticulum Stress-
797 Related Genes in the Middle Frontal Cortex of Subjects with Autism Spectrum Disorder. Mol
798 Neuropsychiatry. 2017;3(2):85-91.
799 62. Ii Timberlake M, Dwivedi Y. Linking unfolded protein response to inflammation and
800 depression: potential pathologic and therapeutic implications. Mol Psychiatry. 2019;24(7):987-
801 94.
802 63. Kelleher III RJ, Bear MF. The autistic neuron: troubled translation? Cell.
803 2008;135(3):401-6.
804 64. Stamova B, Ander BP, Barger N, Sharp FR, Schumann CM. Specific regional and age-
805 related small noncoding RNA expression patterns within superior temporal gyrus of typical

806 human brains are less distinct in autism brains. Journal of child neurology. 2015;30(14):1930-
807 46.
808 65. Chow ML, Pramparo T, Winn ME, Barnes CC, Li H-R, Weiss L, et al. Age-dependent
809 brain gene expression and copy number anomalies in autism suggest distinct pathological
810 processes at young versus mature ages. PLoS Genet. 2012;8(3):e1002592.
811 66. Hashemi E, Ariza J, Rogers H, Noctor SC, Martínez-Cerdeño V. The number of
812 parvalbumin-expressing interneurons is decreased in the prefrontal cortex in autism. Cerebral
813 cortex. 2017;27(3):1931-43.
814 67. Blatt GJ, Fitzgerald CM, Guptill JT, Booker AB, Kemper TL, Bauman ML. Density and
815 distribution of hippocampal neurotransmitter receptors in autism: an autoradiographic study.
816 Journal of autism and developmental disorders. 2001;31(6):537-43.
817 68. Oblak AL, Gibbs TT, Blatt GJ. Reduced GABAA receptors and benzodiazepine binding
818 sites in the posterior cingulate cortex and fusiform gyrus in autism. Brain research.
819 2011;1380:218-28.
820 69. Oblak AL, Gibbs TT, Blatt GJ. Decreased GABAB receptors in the cingulate cortex and
821 fusiform gyrus in autism. Journal of neurochemistry. 2010;114(5):1414-23.
822 70. Oblak A, Gibbs T, Blatt G. Decreased GABAA receptors and benzodiazepine binding
823 sites in the anterior cingulate cortex in autism. Autism Research. 2009;2(4):205-19.
824 71. Qureshi T, Sørensen C, Berghuis P, Jensen V, Dobszay MB, Farkas T, et al. The
825 glutamine transporter Slc38a1 regulates GABAergic neurotransmission and synaptic plasticity.
826 Cerebral Cortex. 2019;29(12):5166-79.
827 72. Jin L-W, Horiuchi M, Wulff H, Liu X-B, Cortopassi GA, Erickson JD, et al. Dysregulation
828 of glutamine transporter SNAT1 in Rett syndrome microglia: a mechanism for mitochondrial
829 dysfunction and neurotoxicity. Journal of Neuroscience. 2015;35(6):2516-29.
830 73. Walle LV, Lamkanfi M, Vandenabeele P. The mitochondrial serine protease HtrA2/Omi:
831 an overview. Cell Death & Differentiation. 2008;15(3):453-60.

832 74. Su XJ, Huang L, Qu Y, Mu D. Progress in research on the role of Omi/HtrA2 in
833 neurological diseases. Reviews in the Neurosciences. 2019;30(3):279-87.
834 75. Kawada K, Kuramoto N, Mimori S. Possibility that the Onset of Autism Spectrum
835 Disorder is Induced by Failure of the Glutamine-Glutamate Cycle. Current molecular
836 pharmacology. 2021;14(2):170-4.
837 76. Wang D, Liu S, Warrell J, Won H, Shi X, Navarro FCP, et al. Comprehensive functional
838 genomic resource and integrative model for the human brain. Science. 2018;362(6420).
839 77. Pirooznia M, Wang T, Avramopoulos D, Valle D, Thomas G, Huganir RL, et al.
840 SynaptomeDB: an ontology-based knowledgebase for synaptic genes. Bioinformatics.
841 2012;28(6):897-9.
842 78. Turner TN, Yi Q, Krumm N, Huddleston J, Hoekzema K, F Stessman HA, et al. denovo-
843 db: a compendium of human de novo variants. Nucleic Acids Res. 2017;45(D1):D804-D11.
844 79. Iossifov I, Levy D, Allen J, Ye K, Ronemus M, Lee Y-H, et al. Low load for disruptive
845 mutations in autism genes and their biased transmission. Proc Natl Acad Sci U S A.
846 2015;112(41):E5600-7.
847 80. Darnell JC, Van Driesche SJ, Zhang C, Hung KYS, Mele A, Fraser CE, et al. FMRP
848 stalls ribosomal translocation on mRNAs linked to synaptic function and autism. Cell.
849 2011;146(2):247-61.
850 81. Oldham MC, Langfelder P, Horvath S. Network methods for describing sample
851 relationships in genomic datasets: application to Huntington's disease. BMC Syst Biol.
852 2012;6:63.
853 82. Love MI, Huber W, Anders S. Moderated estimation of fold change and dispersion for
854 RNA-seq data with DESeq2. Genome biology. 2014;15(12):1-21.
855 83. Li YI, Knowles DA, Humphrey J, Barbeira AN, Dickinson SP, Im HK, et al. Annotation-
856 free quantification of RNA splicing using LeafCutter. Nature genetics. 2018;50(1):151-8.

857 84. Raudvere U, Kolberg L, Kuzmin I, Arak T, Adler P, Peterson H, et al. g: Profiler: a web
858 server for functional enrichment analysis and conversions of gene lists (2019 update). Nucleic
859 acids research. 2019;47(W1):W191-W8.
860 85. Yu G, Wang L-G, Han Y, He Q-Y. clusterProfiler: an R package for comparing biological
861 themes among gene clusters. Omics: a journal of integrative biology. 2012;16(5):284-7.
862 86. Krämer A, Green J, Pollard Jr J, Tugendreich S. Causal analysis approaches in
863 ingenuity pathway analysis. Bioinformatics. 2014;30(4):523-30.
864 87. Skene NG, Grant SG. Identification of vulnerable cell types in major brain disorders
865 using single cell transcriptomes and expression weighted cell type enrichment. Frontiers in
866 neuroscience. 2016;10:16.
867 88. Lake BB, Chen S, Sos BC, Fan J, Kaeser GE, Yung YC, et al. Integrative single-cell
868 analysis of transcriptional and epigenetic states in the human adult brain. Nature biotechnology.
869 2018;36(1):70-80.
870 89. Finucane HK, Bulik-Sullivan B, Gusev A, Trynka G, Reshef Y, Loh P-R, et al. Partitioning
871 heritability by functional annotation using genome-wide association summary statistics. Nature
872 genetics. 2015;47(11):1228-35.

873

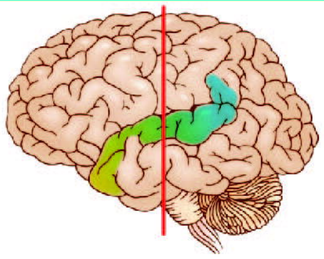

Superior temporal gyrus sampled from 32 Controls 27 ASD

1

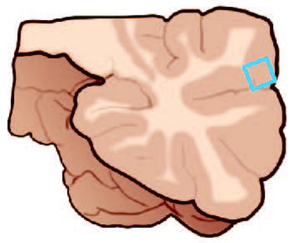

Tissue flash frozen in liquid N_2

2

Ground tissue for bulk analysis

3A

Embedded in OCT for LCM

3B

Sectioned on cryostat to 12 µm

3C

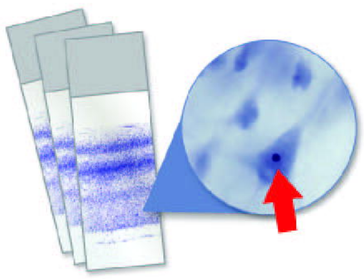

Placed on PEN membrane slides and stained with HistoGene

3D

Neurons (100/sample) captured directly into tubes by laser capture microscope

3E

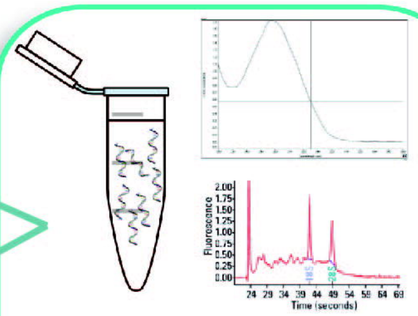

Total RNA extraction and QC

4

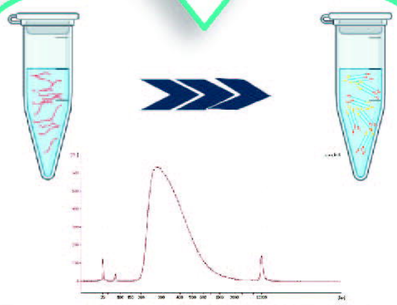

Prepare cDNA libraries, QC, and pool

5

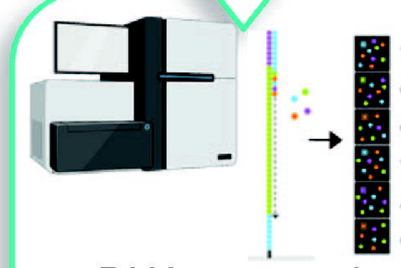

DNA sequencing (50M paired-end 150 bp reads)

6

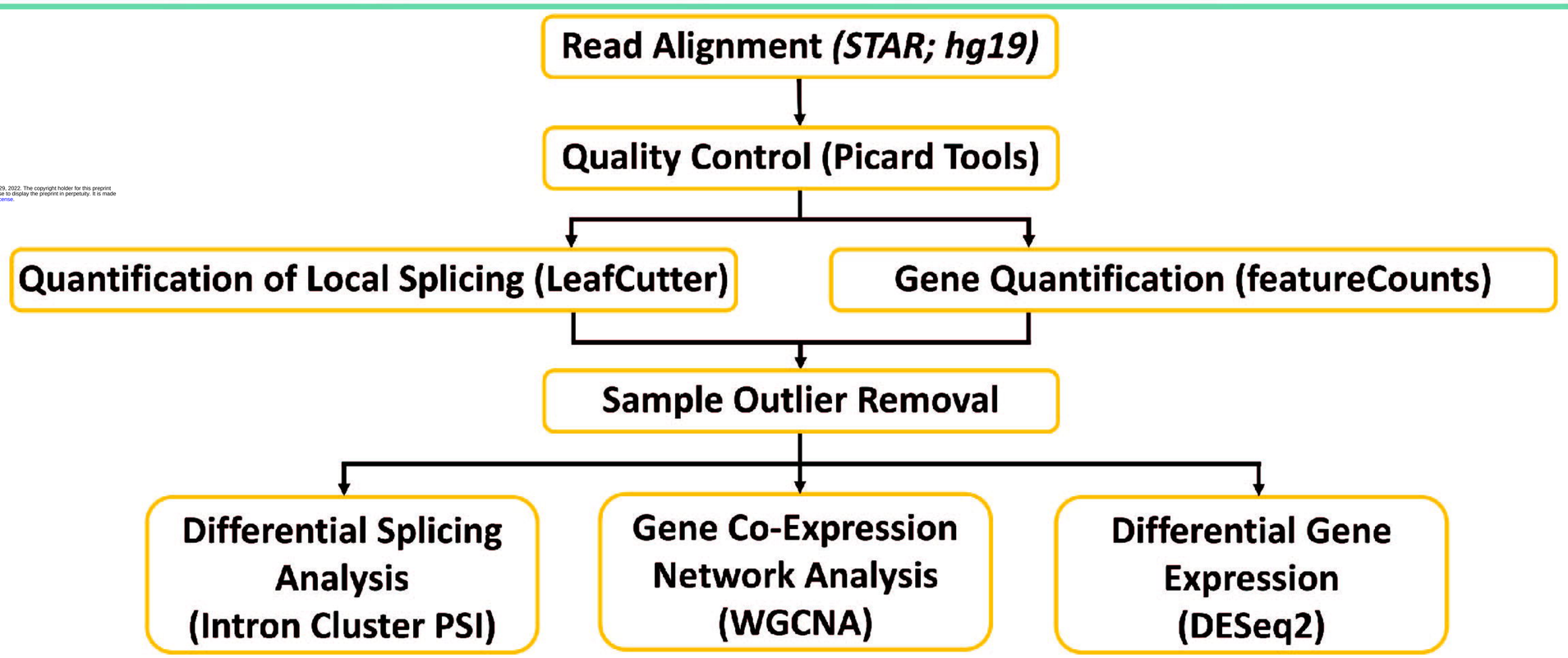

7 Data analysis pipeline

A

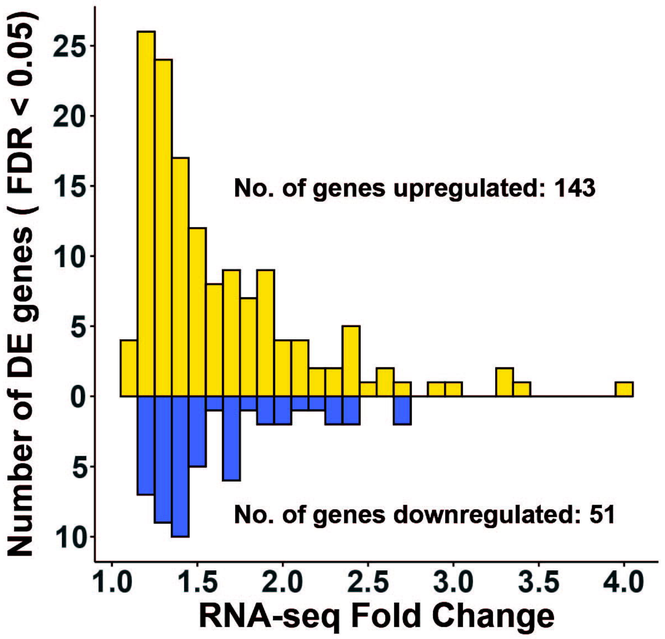
Number of DE genes (FDR < 0.05)
No. of genes upregulated: 143
No. of genes downregulated: 51
RNA-seq Fold Change

B

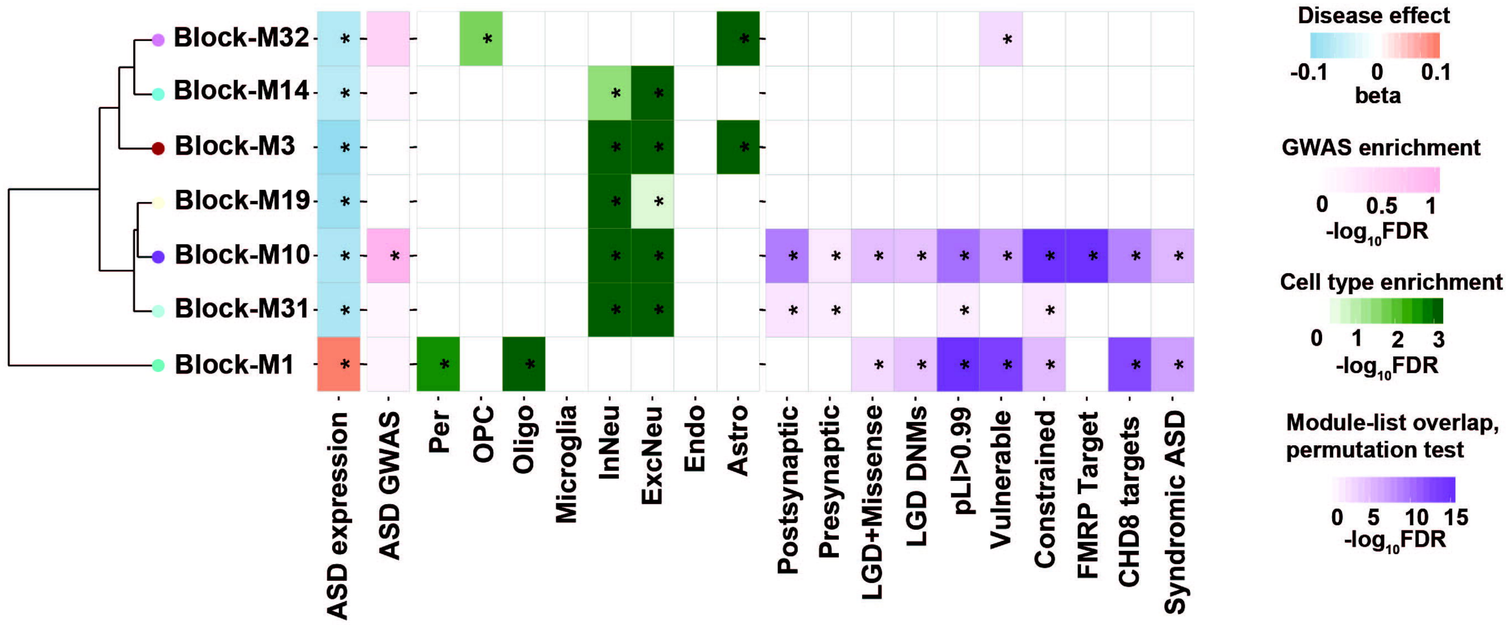
Block-M32
Block-M14
Block-M3
Block-M19
Block-M10
Block-M31
Block-M1
ASD expression
ASD GWAS
Per
OPC
Oligo
Microglia
InNeu
ExcNeu
Endo
Astro
Postsynaptic
Presynaptic
LGD+Missense
LGD DNMs
pLI>0.99
Vulnerable
Constrained
FMRP Target
CHD8 targets
Syndromic ASD
Disease effect
-0.1 0 0.1
beta
GWAS enrichment
0 0.5 1
-log10FDR
Cell type enrichment
0 1 2 3
-log10FDR
Module-list overlap, permutation test
0 5 10 15
-log10FDR

C

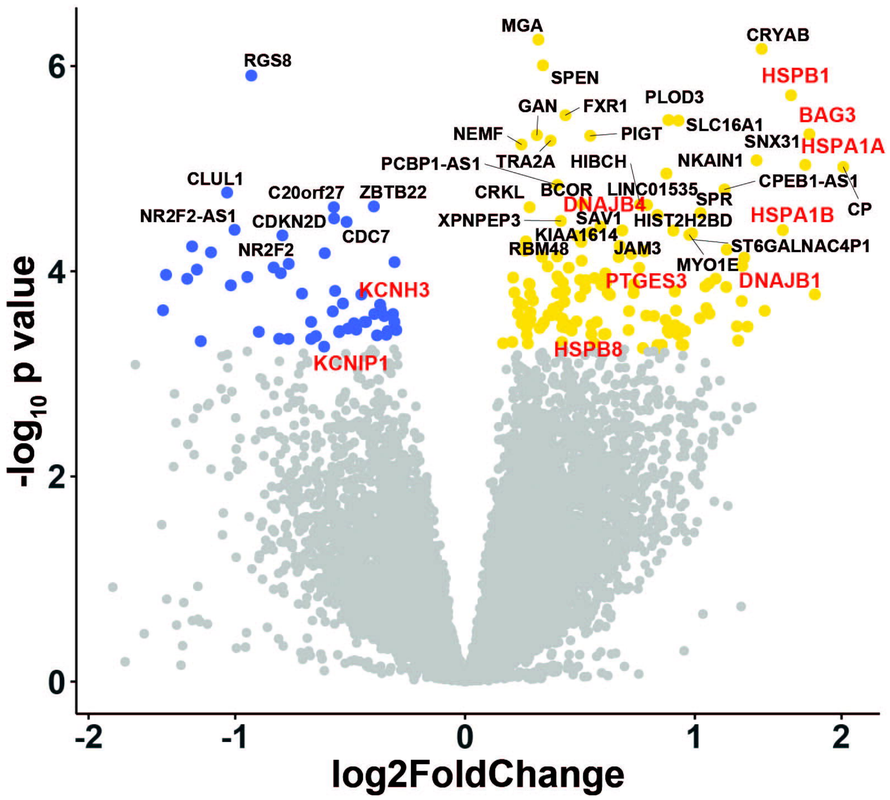
-log10 p value
log2FoldChange
MGA
CRYAB
RGS8
SPEN
HSPB1
PLOD3
GAN
FXR1
BAG3
SLC16A1
NEMF
PIGT
SNX31
HSPA1A
PCBP1-AS1
TRA2A
HIBCH
NKAIN1
CLUL1
CPEB1-AS1
C20orf27
ZBTB22
CRKL
BCOR
LINC01535
SPR
DNAJB4
NR2F2-AS1
CDKN2D
XPNPEP3
SAV1
HIST2H2BD
HSPA1B
CP
CDC7
KIAA1614
NR2F2
RBM48
JAM3
ST6GALNAC4P1
MYO1E
KCNH3
PTGES3
DNAJB1
HSPB8
KCNIP1

D

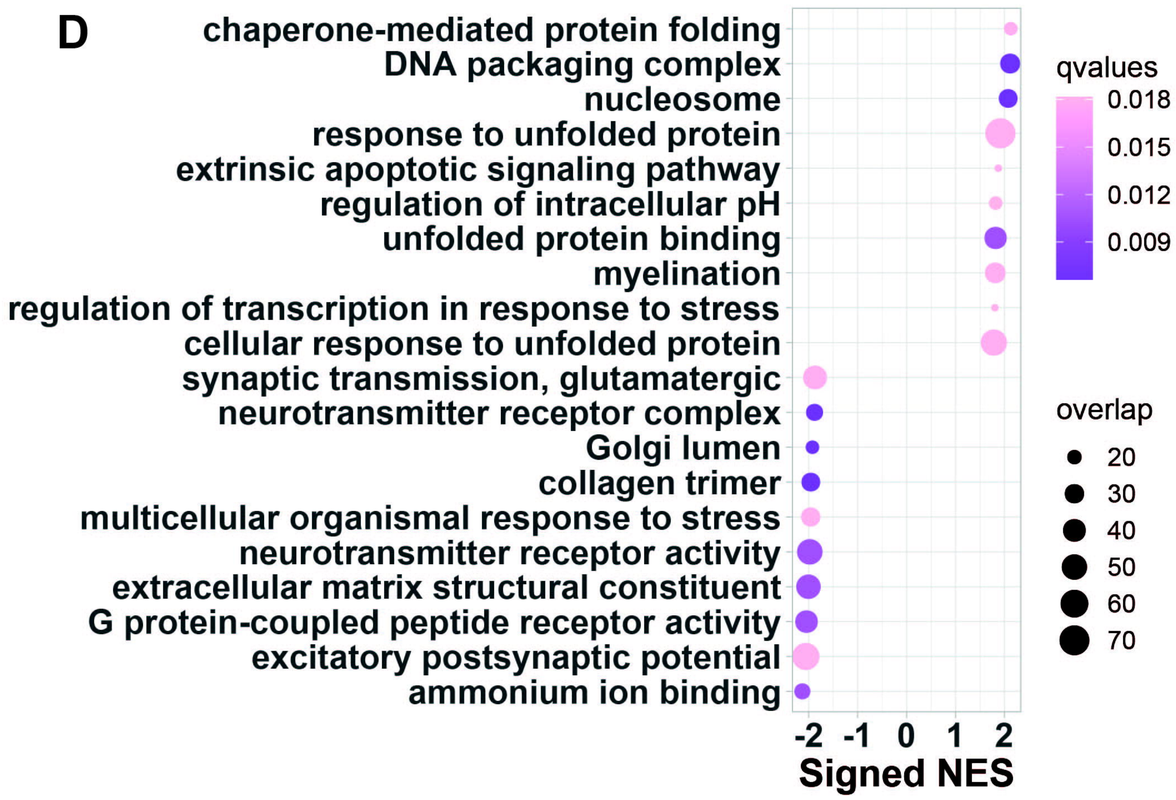
chaperone-mediated protein folding
DNA packaging complex
nucleosome
response to unfolded protein
extrinsic apoptotic signaling pathway
regulation of intracellular pH
unfolded protein binding
myelination
regulation of transcription in response to stress
cellular response to unfolded protein
synaptic transmission, glutamatergic
neurotransmitter receptor complex
Golgi lumen
collagen trimer
multicellular organismal response to stress
neurotransmitter receptor activity
extracellular matrix structural constituent
G protein-coupled peptide receptor activity
excitatory postsynaptic potential
ammonium ion binding
Signed NES
qvalues
0.018
0.015
0.012
0.009
overlap
20
30
40
50
60
70

E

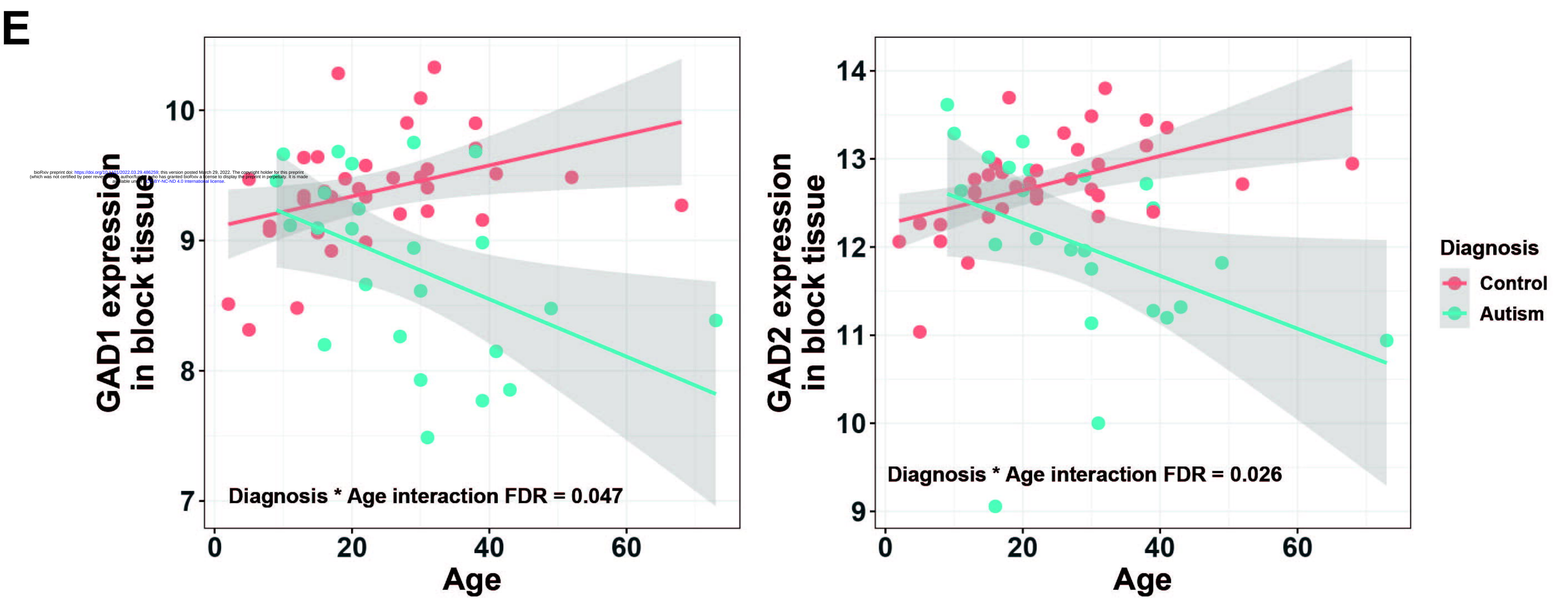
GAD1 expression in block tissue
Diagnosis * Age interaction FDR = 0.047
Age
GAD2 expression in block tissue
Diagnosis * Age interaction FDR = 0.026
Age
Diagnosis
Control
Autism

F

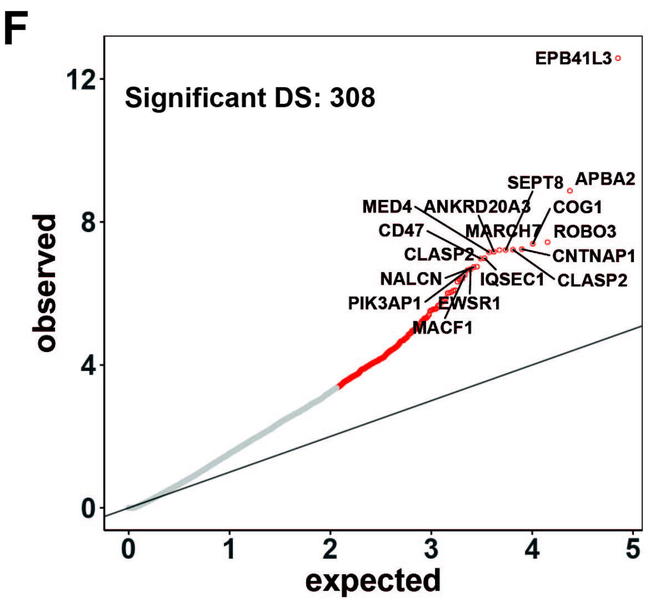
Significant DS: 308
observed
expected
EPB41L3
SEPT8
APBA2
MED4
ANKRD20A3
COG1
CD47
MARCH7
ROBO3
CLASP2
CNTNAP1
NALCN
IQSEC1
CLASP2
PIK3AP1
EWSR1
MACF1

A

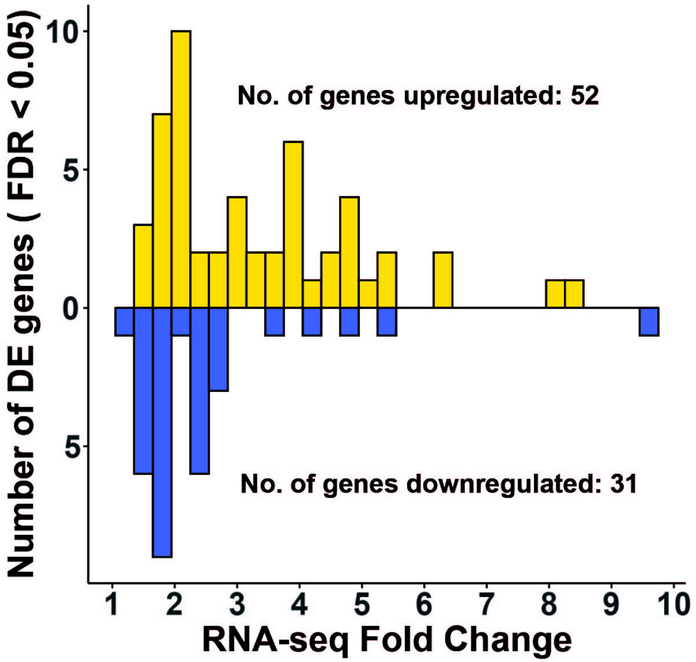

B

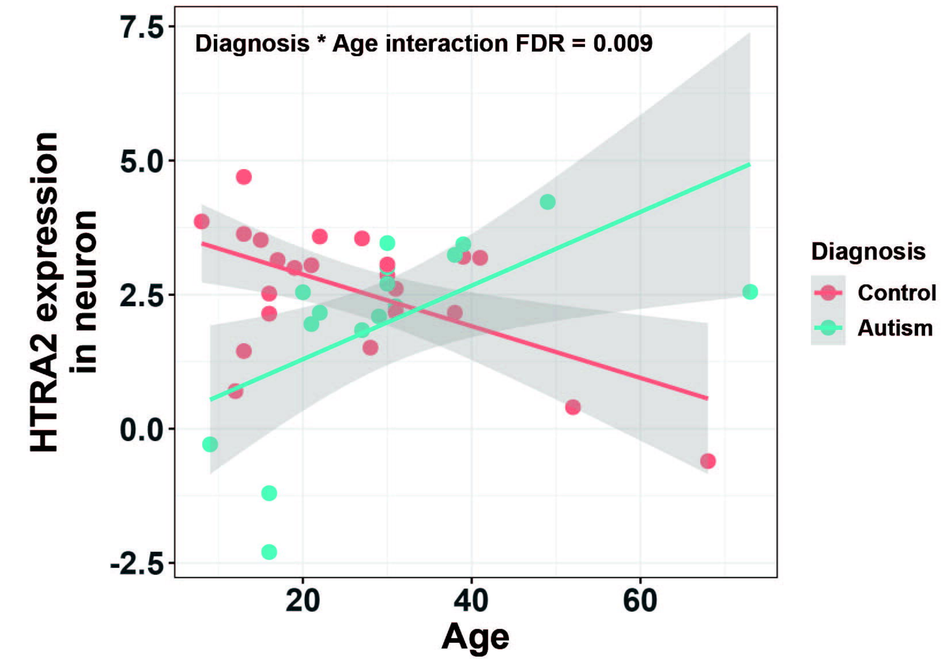

C

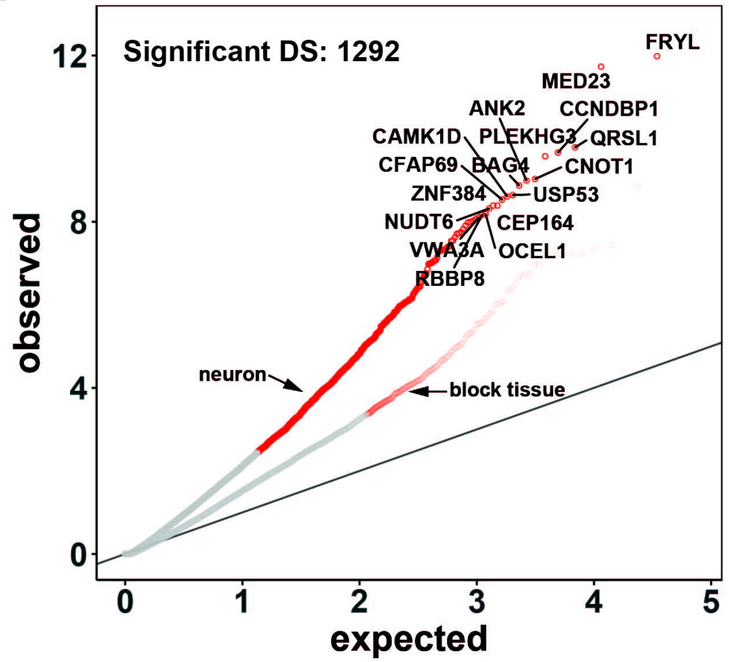

D

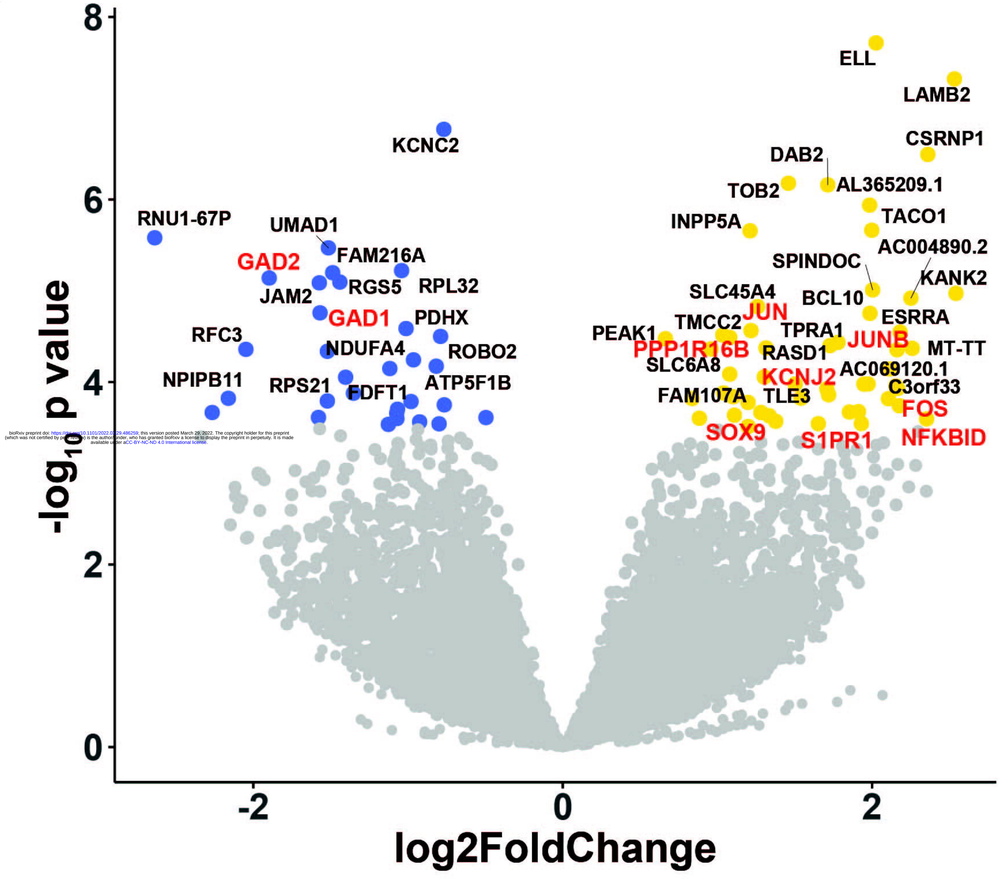

E

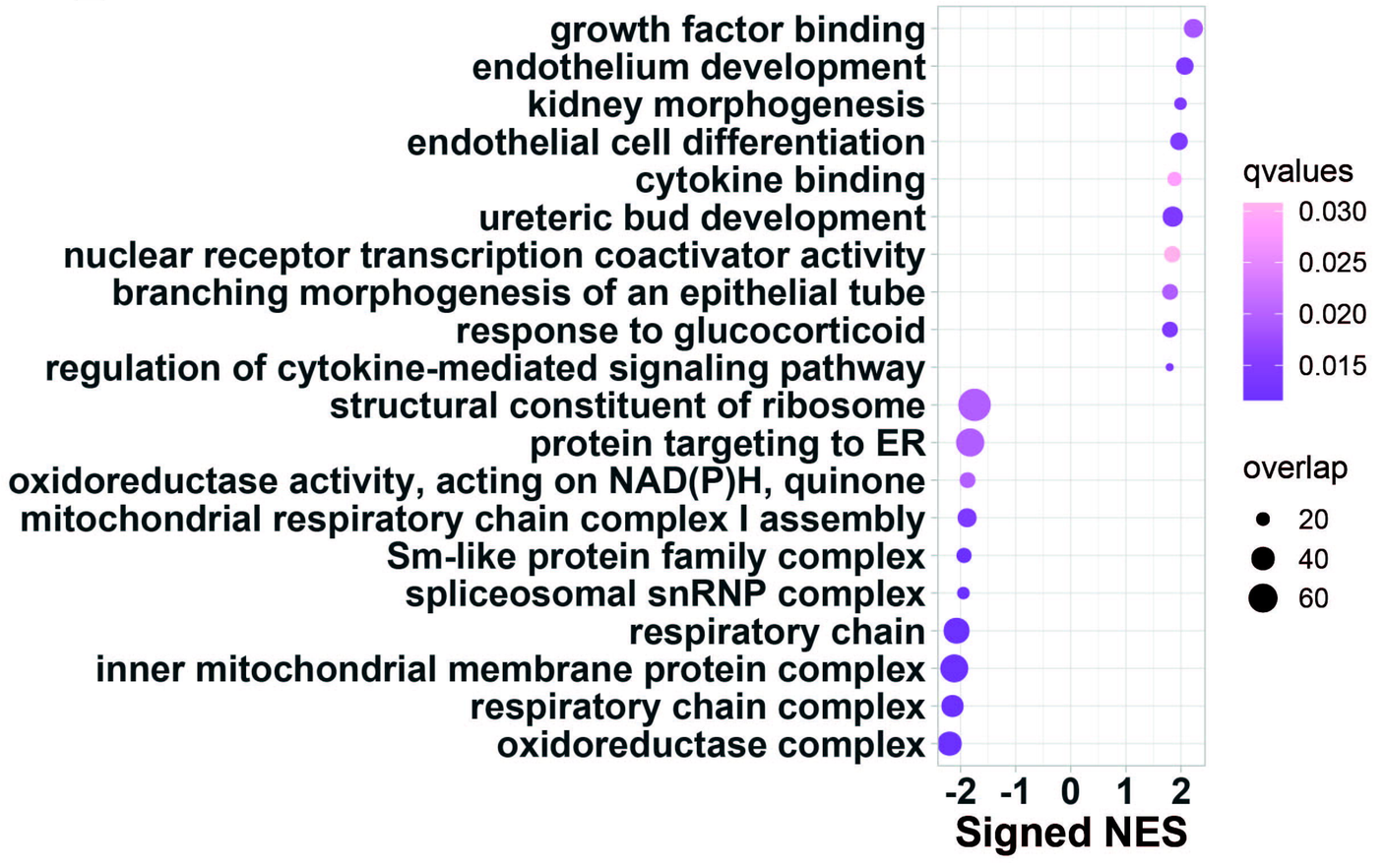

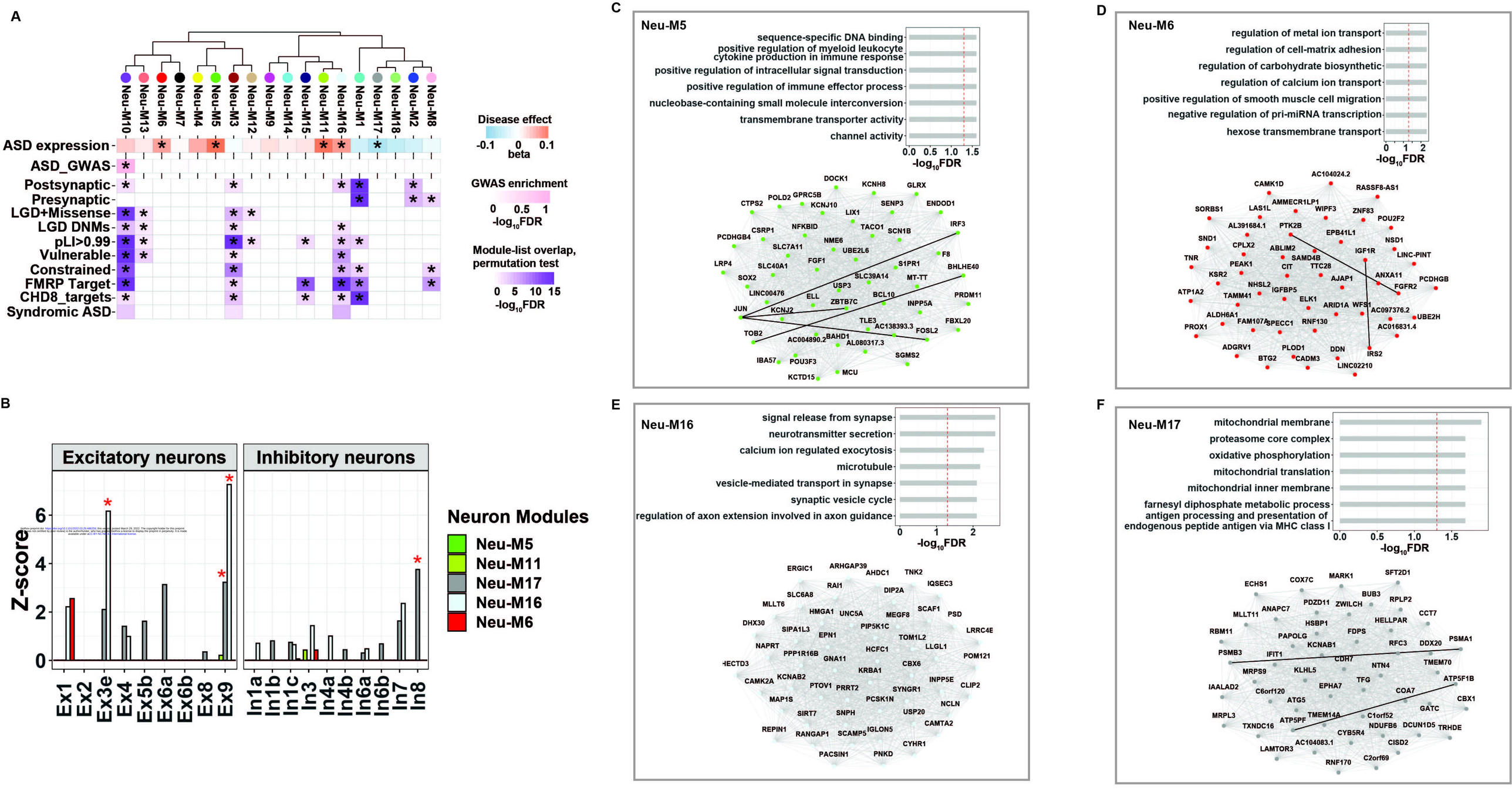
A
Neu-M10
Neu-M13
Neu-M6
Neu-M7
Neu-M4
Neu-M5
Neu-M3
Neu-M12
Neu-M9
Neu-M14
Neu-M15
Neu-M11
Neu-M16
Neu-M1
Neu-M17
Neu-M18
Neu-M2
Neu-M8
ASD expression
ASD_GWAS
Postsynaptic
Presynaptic
LGD+Missense
LGD DNMs
pLI>0.99
Vulnerable
Constrained
FMRP Target
CHD8_targets
Syndromic ASD
Disease effect
-0.1 0 0.1
beta
GWAS enrichment
0 0.5 1
-log10FDR
Module-list overlap, permutation test
0 5 10 15
-log10FDR
B
Excitatory neurons
Inhibitory neurons
Z-score
Ex1 Ex2 Ex3e Ex4 Ex5b Ex6a Ex6b Ex8 Ex9
In1a In1b In1c In3 In4a In4b In6a In6b In7 In8
Neuron Modules
Neu-M5
Neu-M11
Neu-M17
Neu-M16
Neu-M6
C
Neu-M5
sequence-specific DNA binding
positive regulation of myeloid leukocyte cytokine production in immune response
positive regulation of intracellular signal transduction
positive regulation of immune effector process
nucleobase-containing small molecule interconversion
transmembrane transporter activity
channel activity
0.0 0.5 1.0 1.5
-log10FDR
DOCK1
KCNH8
GLRX
CTPS2
POLD2
GPRC5B
KCNJ10
LIX1
SENP3
ENDOD1
CSRP1
NFKBID
TACO1
SCN1B
IRF3
PCDHGB4
NME6
SLC7A11
UBE2L6
F8
LRP4
SLC40A1
FGF1
S1PR1
BHLHE40
SOX2
SLC39A14
MT-TT
LINC00476
USP3
ELL
BCL10
PRDM11
JUN
KCNJ2
ZBTB7C
INPP5A
TLE3
AC138393.3
FBXL20
TOB2
AC004890.2
BAHD1
AL080317.3
FOSL2
SGMS2
IBA57
POU3F3
MCU
KCTD15
D
Neu-M6
regulation of metal ion transport
regulation of cell-matrix adhesion
regulation of carbohydrate biosynthetic
regulation of calcium ion transport
positive regulation of smooth muscle cell migration
negative regulation of pri-miRNA transcription
hexose transmembrane transport
0 1 2
-log10FDR
AC104024.2
CAMK1D
RASSF8-AS1
SORBS1
LAS1L
AMMECR1LP1
WIPF3
ZNF83
POU2F2
AL391684.1
PTK2B
EPB41L1
SND1
CPLX2
ABLIM2
NSD1
IGF1R
TNR
SAMD4B
LINC-PINT
PEAK1
CIT
TTC28
KSR2
AJAP1
ANXA11
PCDHGB
NHSL2
IGFBP5
FGFR2
ATP1A2
TAMM41
ELK1
ARID1A
WFS1
AC097376.2
ALDH6A1
FAM107A
SPECC1
RNF130
UBE2H
PROX1
AC016831.4
ADGRV1
PLOD1
DDN
IRS2
BTG2
CADM3
LINC02210
E
Neu-M16
signal release from synapse
neurotransmitter secretion
calcium ion regulated exocytosis
microtubule
vesicle-mediated transport in synapse
synaptic vesicle cycle
regulation of axon extension involved in axon guidance
0 1 2
-log10FDR
ERGIC1
ARHGAP39
AHDC1
TNK2
RAI1
IQSEC3
DIP2A
SLC6A8
MLLT6
HMGA1
UNC5A
MEGF8
SCAF1
PSD
DHX30
SIPA1L3
PIP5K1C
LRRC4E
EPN1
TOM1L2
NAPRT
HCFC1
LLGL1
PPP1R16B
GNA11
POM121
HECTD3
CBX6
KRBA1
CAMK2A
KCNAB2
INPP5E
CLIP2
PTOV1
PRRT2
SYNGR1
MAP1S
PCSK1N
NCLN
SIRT7
SNPH
USP20
CAMTA2
REPIN1
RANGAP1
SCAMP5
IGLON5
CYHR1
PACSIN1
PNKD
F
Neu-M17
mitochondrial membrane
proteasome core complex
oxidative phosphorylation
mitochondrial translation
mitochondrial inner membrane
farnesyl diphosphate metabolic process
antigen processing and presentation of endogenous peptide antigen via MHC class I
0.0 0.5 1.0 1.5
-log10FDR
ECHS1
COX7C
MARK1
SFT2D1
BUB3
RPLP2
PDZD11
ZWILCH
ANAPC7
CCT7
MLLT11
HSBP1
HELLPAR
RBM11
PAPOLG
FDPS
KCNAB1
RFC3
DDX20
PSMA1
PSMB3
IFIT1
CDH7
TMEM70
NTN4
MRPS9
KLHL5
ATP5F1B
IAALAD2
C6orf120
EPHA7
TFG
COA7
CBX1
ATG5
GATC
MRPL3
ATP5PF
TMEM14A
C1orf52
TXNDC16
NDUFB6
DCUN1D5
TRHDE
CYB5R4
AC104083.1
CISD2
LAMTOR3
RNF170
C2orf69

A

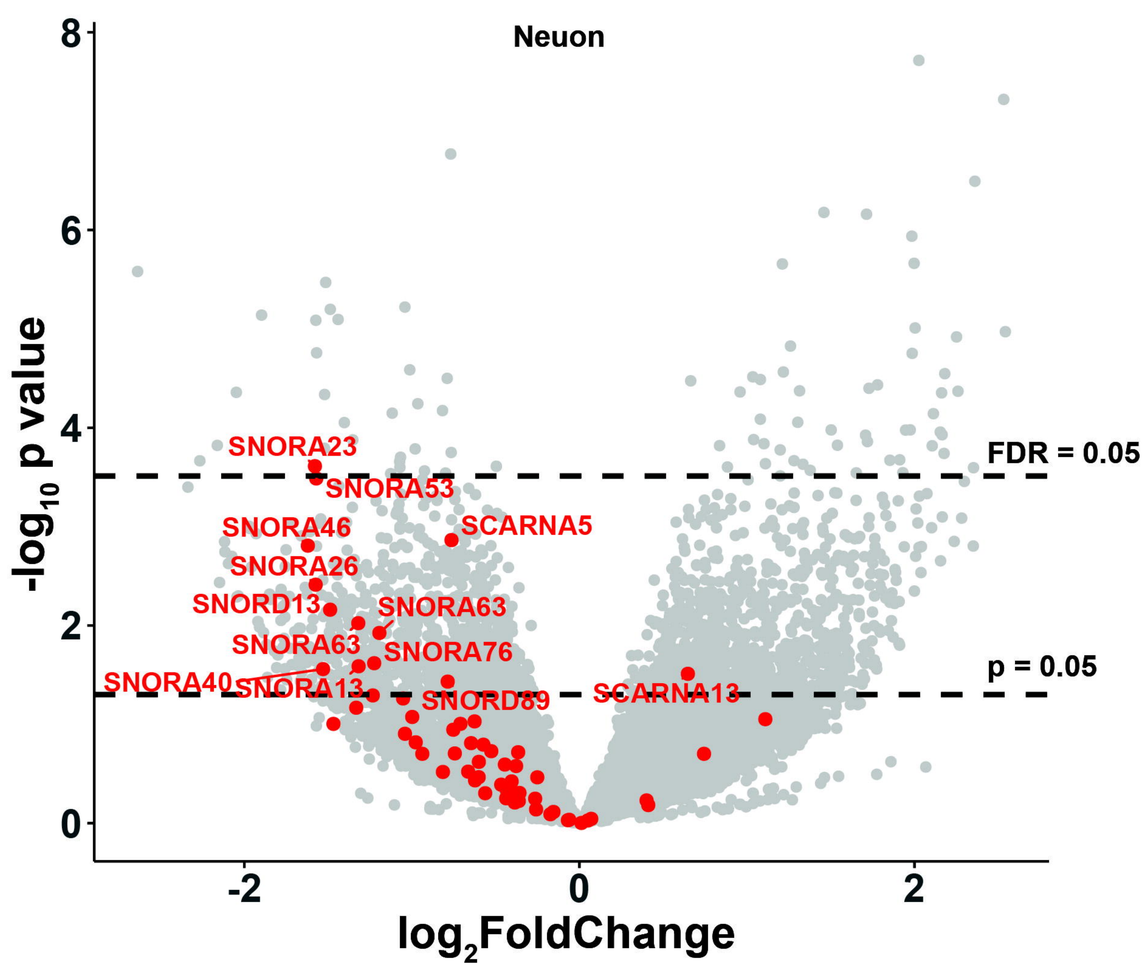
Neuon
-log10 p value
log2FoldChange
FDR = 0.05
p = 0.05
SNORA23
SNORA53
SNORA46
SCARNA5
SNORA26
SNORD13
SNORA63
SNORA63
SNORA76
SNORA40
SNORA13
SNORD89
SCARNA13

B

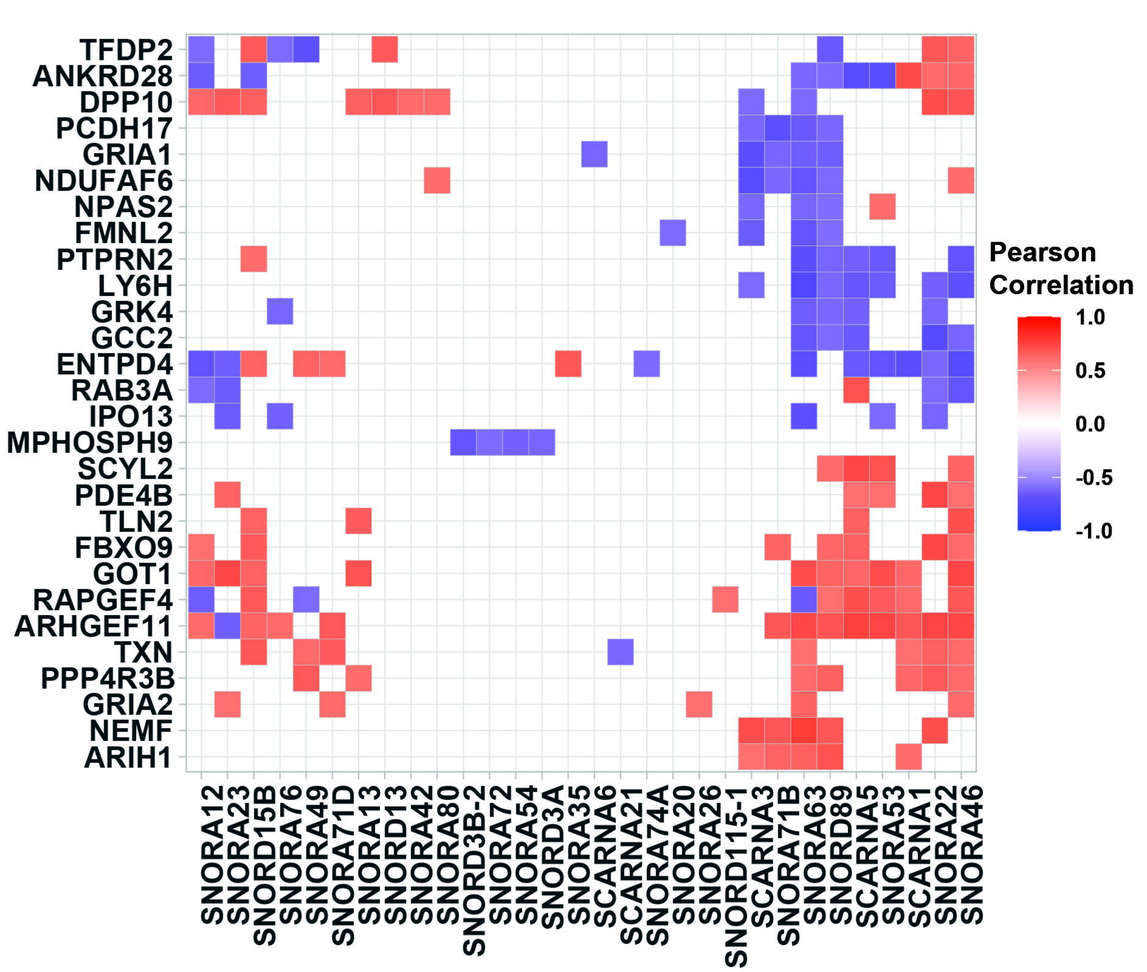
TFDP2
ANKRD28
DPP10
PCDH17
GRIA1
NDUFAF6
NPAS2
FMNL2
PTPRN2
LY6H
GRK4
GCC2
ENTPD4
RAB3A
IPO13
MPHOSPH9
SCYL2
PDE4B
TLN2
FBXO9
GOT1
RAPGEF4
ARHGEF11
TXN
PPP4R3B
GRIA2
NEMF
ARIH1
SNORA12
SNORA23
SNORD15B
SNORA76
SNORA49
SNORA71D
SNORA13
SNORD13
SNORA42
SNORA80
SNORD3B-2
SNORA72
SNORA54
SNORD3A
SNORA35
SCARNA6
SCARNA21
SNORA74A
SNORA20
SNORA26
SNORD115-1
SCARNA3
SNORA71B
SNORA63
SNORD89
SCARNA5
SNORA53
SCARNA1
SNORA22
SNORA46
Pearson Correlation
1.0
0.5
0.0
-0.5
-1.0

C

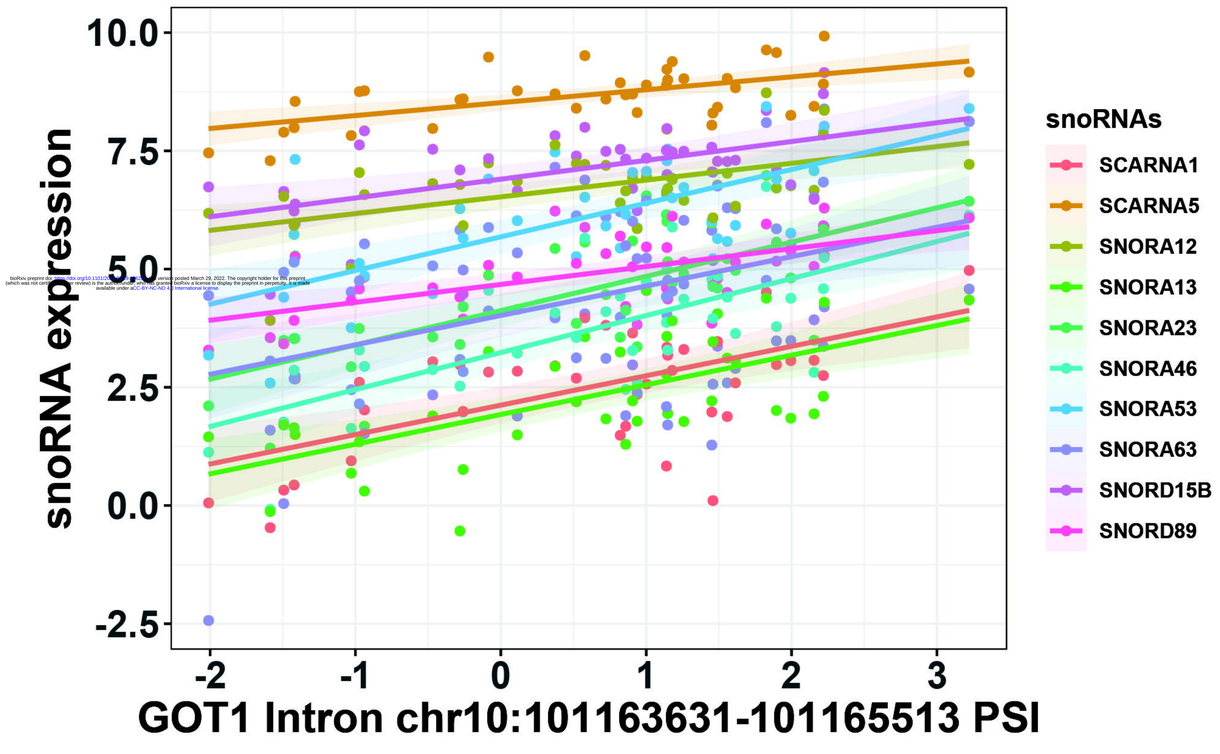
snoRNA expression
GOT1 Intron chr10:101163631-101165513 PSI
snoRNAs
SCARNA1
SCARNA5
SNORA12
SNORA13
SNORA23
SNORA46
SNORA53
SNORA63
SNORD15B
SNORD89

D

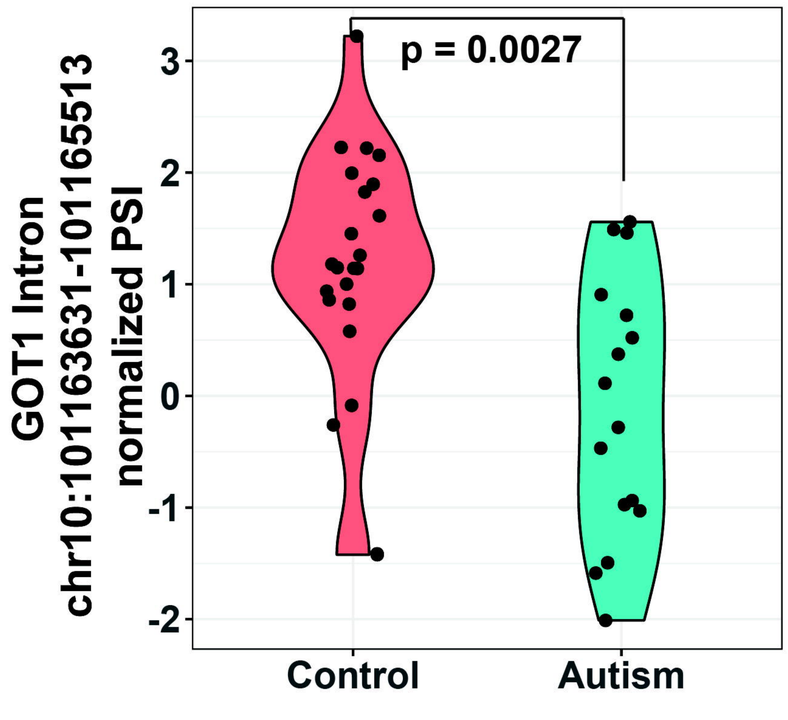
GOT1 Intron chr10:101163631-101165513 normalized PSI
p = 0.0027
Control
Autism